Interlaboratory Comparison An International Intercomparison of

Continuous Flow Analysis (CFA) Systems for High-Resolution Water Isotope Measurements in Ice Cores

Agnese Petteni^{1,2}, Elise Fourré², Elsa Gautier³, Azzurra Spagnesi^{4,1}, Roxanne Jacob², Pete D. Akers^{3,5}, Daniele Zannoni¹, Jacopo Gabrieli⁴, Olivier Jossoud², Frédéric Prié², Amaëlle Landais², Titouan Tcheng², Barbara Stenni¹, Joel Savarino³, Patrick Ginot³, Mathieu Casado²

¹Ca' Foscari of Venice, Department of Environmental Sciences, Informatics and Statistics, Mestre (Venice), Italy

Correspondence to: Agnese Petteni (agnese.petteni@unive.it)

Abstract. The Continuous Flow Analysis technique coupled with Cavity Ring Down Spectrometry (CFA-CRDS) provides a method for high-resolution water isotope analysis of ice cores, which is essential for paleoclimatic reconstructions of local temperatures and regional atmospheric circulation. Compared to the traditional discrete method, CFA-CRDS significantly reduces analysis time. However, the effective resolution at which the isotopic signal can be retrieved from continuous measurements is influenced by system-induced mixing, which smooths the isotopic signal, and by measurement noise, which can further limit the resolution of the continuous record introducing random fluctuations in the instrument's signal output. This study compares three CFA-CRDS systems developed at the Institute of Polar Science, National Research Council, in collaboration with Ca' Foscari University (Venice), the Laboratoire des Sciences du Climat et de l'Environnement (Paris), and the Institut des Géosciences de l'Environnement (Grenoble) for firm core analysis. Continuous results are compared with discrete data to highlight the strengths and limitations of each system. A spectral analysis is also performed to quantify the impact of internal mixing on signal integrity and to determine the frequency limits imposed by measurement noise. These findings establish the effective resolution limits for retrieving isotopic signals from firn cores. Finally, we discuss critical system configurations and procedural optimizations that enhance the accuracy and resolution of water isotope analysis in ice cores.

1 Introduction

Water isotopes are valuable proxies for studying past climatic processes, providing insights into local temperature and atmospheric circulation patterns (Dansgaard, 1964; Petit et al., 1999). In permanently frozen regions of Antarctica, the glacial ice sampled through ice coring serves as a continuous archive of past climate conditions, with annual snowfall creating new layers at the top of the ice sheet every year. Low-accumulation areas like the East Antarctic Plateau (20-50-75 mm weg yr⁻¹,

²LSCE/IPSL, CEA-CNRS-UVSQ, Université Paris-Saclay, Gif-sur-Yvette, France

³Université Grenoble Alpes, CNRS, IRD, Grenoble INP, INRAE, IGE, F-38000 Grenoble, France

O 4Institute of Polar Sciences, National Research Council of Italy, Venice, Italy

⁵Geography, School of Natural Sciences, Trinity College Dublin, Ireland

Landais et al., 2017; Wesche et al., 2016) often yield records with decadal or multi-decadal resolution (Casado et al., 2020; Petit, 1982). By contrast, in high-accumulation areas (100-300 mm weq yr⁻¹), such as coastal regions in East Antarctica and West Antarctica, ice core records can achieve seasonal or annual resolution (Alley, 2000; Markle et al., 2017; Sigl et al., 2016). Depositional processes, such as precipitation intermittency (Casado et al., 2020; Laepple et al., 2011; Steig, 1994), introduces bias into the snow layers' recorded signal. In addition, post-depositional processes, including wind-driven snow redistribution (Picard et al., 2019), sublimation, and condensation, introduce stratigraphic noise into the snow's surface composition and alter local surface values (Casado et al., 2021; Wahl, 2022). Meanwhile, isotopic composition below the surface can be modified over time through processes like diffusion (Genthon et al., 2017). The deformation of deeper ice layers under the weight of the ice sheet compresses the timescale retrieved from each centimetre of ice analysed (Huybrechts et al., 2007). Therefore, high-resolution analyses are critical for ice cores to preserve the integrity of the isotopic signal. While deep ice cores from low-accumulation areas are traditionally analysed using discrete sampling with resolution ranging from 10 cm to 50 cm (Grisart et al., 2022; Amaëlle Landais & Stenni, 2021), higher resolution (< 10 cm) is achieved in cores from highaccumulation areas, where seasonal signal can be detected (Crotti et al., 2022; Goursaud et al., 2017). In both cases, although precise, this method is time-consuming due to the extensive sample preparation and the need for offline analysis. In contrast, Continuous Flow Analysis (CFA) coupled with a Cavity Ring-Down Spectrometer (CRDS) has emerged as a more efficient alternative, enabling high-resolution measurements of water isotopes (Gkinis et al., 2010). This system slowly and continuously melts solid ice sticks at the base, with the resulting liquid water directed into a vaporiser before being injected into a CRDS instrument - typically a Picarro-brand isotopic analyser. This method eliminates the need for manual sample handling, significantly reducing analysis time. For instance, within the East Antarctic International Ice Sheet Traverse (EAIIST - (Traversa et al., 2023) project, the analysis of 18 firm cores collected on the Antarctic Plateau (total length of about 960 m) would results in analysing approximately 20,000 samples at resolution of 5 cm. This would take more than two years of discrete analysis if conducted with a single CRDS instrument. In contrast, with CFA-CRDS, operating at a melt rate of 2.5-3 cm min⁻¹, the same analysis can be completed in roughly three months, with the capability to process up to 10 meters of ice core per day. Additionally, the CFA offers the great advantage of providing - in parallel to the line for isotopic analysis a non-contaminated innermost melt water flow for further analysis. The innermost melt water flow is used for direct measurement, such as chemical analysis (trace elements, heavy metals, biomass burning tracers, etc.), and insoluble particle volume and distribution, and is simultaneously collected as discrete aliquots, greatly reducing the need for decontamination procedures in clean room. Despite its advantages, CFA-CRDS faces several-some technical limitations for isotopic analysis, one being the mixing of water molecules within the system, leading to signal smoothing (Gkinis et al., 2011). We use the term "mixing", following the definition of Jones et al., (2017a) for all the smoothing effects on the signal that occur within the CFA-CRDS system, including mixing occurring from the melt-head to the instrument cavity. Mixing may decrease the signal amplitude. On the other hand, we refer to "diffusion" for all the attenuation processes that happen naturally with in the firn. Overall, the transfer function of both processes is following the same equation (Eq. 1), but the length is usually longer for diffusion. The mixing length, influenced by technical setup and variations in core section density at the melt-head stage due to capillary action, can differ

significantly between systems. Consequently, isotopic values must be averaged over a depth interval equivalent to the mixing length to ensure accurate representation of the preserved climatic signal within the cores. This mixing ean occur at various stages, from the melt head to the instrument cavity, displacing water molecules from their original relative positions. The extend of this effect can vary with changes in melt rate, especially at the melt head level due to capillary action. As a result, isotopic values must be averaged over a depth range corresponding to the mixing length to accurately represent the preserved elimatic signal (Gkinis et al., 2011; Jones et al., 2017a). Additionally, measurement noise – referring to random fluctuations in the instrument' signal output – further limits the effective resolution, restricting the ability to retrieve meaningful climatic signals at high frequencies. Accurately determining the delay time between the melt head and CRDS signals is critical for converting the timescale to a depth scale. Additionally, issues during core melting, such as temporary blockages or stick collapses, introduce uncertainties when assigning depth to the isotopic profile.

In this study, we present the 4-m section of the firn PALEO2 core (EAIIST), analysed at three research institutes: the Institute of Polar Science, National Research Council, in collaboration with Ca' Foscari University (ISP-UNIVE, Venice, Italy), Laboratoire des Sciences du Climat et de l'Environnement (LSCE, Paris, France), and the Institut des Géosciences de l'Environnement (IGE, Grenoble, France). These laboratories collaborate on international ice core projects such as EAIIST and Beyond EPICA Oldest Ice Core (BE-OIC - Lilien et al., 2021; Parrenin et al., 2017) and share common samples, emphasising the need for accurate comparisons between the different systems. We compared CFA results with discrete profile at 1.5 cm resolution to highlight the strengths and limitations of each technical setup and operating procedure. Power spectral density (PSD) analysis is used to quantify the effects of mixing on the signal and to determine the maximum resolution achievable by each system, as constrained by internal mixing and measurement noise.

5 2 Methods

2.1 Ice Core Processing

Four ice cores were drilled at the PALEO site (79°64'S, 126°13'E, borehole temperature: -46.5 °C) during the EAIIST on the Antarctic Plateau (Traversa et al., 2023). In this study, we focus on the PALEO2 firn core (18 m deep) to compare three CFA-CRDS systems. The full core was continuously analysed at LSCE in June 2023, while 4-m sections (12–16 m depth) were analysed at IGE in July 2023 and at ISP-UNIVE in January 2024. This 4-m interval, with an average density of ~0.58 g cm⁻³, was selected to explore the performance of the systems on low-density firn while maintaining sufficient structural integrity for handling and analysis in the cold room. Here, we use the PALEO2 firn core (18 m) to compare three CFA-CRDS systems. The entire core was continuously analysed at LSCE in June 2023, while 4-m sections (depth 12–16 m) of the same core were analysed at IGE in July 2023 and at ISP-UNIVE in January 2024. This depth interval, with a density of about 0.58 g cm⁻³, was chosen to provide new insights into the analysis of low-density sections of the cores, while ensuring sufficient structural integrity during processing in the cold room. The core was cut into about 1.00x0.03x0.03 m sticks (Fig. 1)_-, with cuts for LSCE and IGE sticks done in June 2023 and for ISP-UNIVE in January 2024. During the preparation of the ice sticks for the

ha formattato: Colore carattere: Automatico

ha formattato: Colore carattere: Automatico

ISP-UNIVE measurements, discrete samples of 1.5 cm length were also cut. However, due to sample loss during the cutting process and uncertainties associated with manual cutting, the discrete samples resulted in a final average resolution of 1.7 cm on average. The samples were stored frozen in PTFE bottles and analysed offline. During the preparation of the ice sticks for the ISP-UNIVE measurements, we also prepared discrete samples with a depth resolution of 1.5 cm, which were stored frozen in PTFE bottles and analysed offline. Spectral analyses (Sect. 3.3, Fig. 8) show no significant diffusion occurred during the six-month storage at -20°C between the two cutting sessions. The comparison between the spectra will be presented in Sect. 3.5, Fig. 8. The remaining quarter of the core was stored in plastic bags for any future investigation.

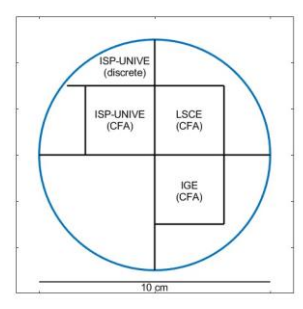


Figure 1. Cutting scheme of PALEO2 core for CFA-CRDS systems and discrete sampling.

2.2 Isotopic Measurements and Data Calibration

The isotope values of δD (or δ^2H) and $\delta^{18}O$ are here reported as the deviation of the ratio of heavy to light isotopes relative to the Vienna Standard Mean Ocean Water (V-SMOW—<u>Tab. 1a</u>) international standard, where δ values are expressed in parts per mil (‰):

 $\delta_{\text{(\%)}} = (R_{\text{SAMPLE}}/R_{\text{VSMOW}}-1)*1000$

where R_{SAMPLE} and R_{VSMOW} are the ratios between ^{18}O / ^{16}O or D/H in the sample and in V-SMOW, respectively. The second-order parameter deuterium excess (d_{xs}) is defined as follows (Craig, 1963; Dansgaard, 1964):

 $d_{xs} = \delta D - 8 x^{*} \delta^{18}O$

100

105

110

120

All reported isotope values are calibrated against the internal laboratory standards (STDs) provided by each institute (Tab. 1), which are in turn calibrated against international reference waters V-SMOW (Vienna Standard Mean Ocean Water – Tab. 1a) and SLAP (Standard Light Antarctic Precipitation – Tab. 1a). Calibration involves applying a linear regression between the "measured" and "known" values of STDs, using the resulting slope and intercept to correct the sample data to the reference scale. Calibration STDs have isotopic compositions similar to those expected for Antarctic ice cores (Landais & Stenni, 2021) to minimize the instrument's memory effect and accurately capture the highly negative isotopic values typical of polar snow.

The discrete samples were analysed at ISP-UNIVE using a Picarro L2140-i. The standards TD (Talos Dome) and AP1 (Antarctic Plateau 1) were used for calibration, while two vials of DCS (Dome C Snow) were analysed as controls (Tab. 1b). The accuracy of offline measurements was determined as the mean difference between control and true values of the STDs controls, with uncertainty represented by their standard deviation (SD). This yielding an accuracy of -0.01 % for δ^{18} O, -0.07 % for δ D, and -0.02 % for d-excess, with corresponding uncertainties of \pm 0.07 %, \pm 0.4 %, and \pm 0.4 %, respectively.

125

130

135

The continuous analyses were conducted using the three CFA systems coupled with CRDS Picarro-brand isotopic analysers: the L2130-i model at ISP-UNIVE and LSCE, and the L2140-i model at IGE. At ISP-UNIVE, a Picarro L2140-i was utilized for the discrete analysis. The standards TD (Talos Dome) and AP1 (Antarctic Plateau 1) were used for calibration, while two yials of DCS (Dome C Snow) were analysed as controls. The accuracy of offline measurements was determined as the mean difference between control and true values of the STDs controls, with uncertainty represented by their SD. This vielding an accuracy of -0.01% for δ^{18} O, -0.07% for δ D, and -0.02% for d-excess, with corresponding uncertainties of ±0.07‰, ±0.4‰, and ±0.4‰, respectively. The three CFA systems discussed in this study are all coupled with CRDS Picarrobrand isotopic analysers. Continuous raw data are calibrated by injecting water STDs at a constant humidity level before and/or after each daily measurement. From each calibration standard injection, only a data interval with stable humidity is selected. At the ISP-UNIVE laboratory, standards AP1 and DCS (Tab. 1b) are injected for 20 minutes, with the final 5 minutes used for analysis. At LSCE, standards NEEM, Adélie, and OC4 (Tab. 1c) are injected for 25 minutes and the final 3 minutes are selected. At IGE, standards EDC, EGRIP-01, and SOUP-01 (Tab. 1d) are injected for 10 minutes and a 3-minute interval with stable humidity is chosen. At ISP-UNIVE laboratory, calibration standards (AP1 and DCS) are injected for 20 min, while the last 5 min are selected to minimise the SD. At LSCE, standards (NEEM, Adelie, and OC4) are injected for 25 min selecting the final 3 min. At IGE, the standards (EDC, EGRIP-01, and SOUP-01) are injected for 10 min and a 3-min interval is selected. At the ISP-UNIVE, STDs are measured at the start of the day, while at LSCE and IGE, STDs are measured both at the beginning and end of the analysis. At LSCE, three calibration methods - using start-day, end-day, or the average of both - were tested, showing no significant measurement drift throughout the day.

Table 1. <u>Isotopic values (%) of a) international standards V-SMOW and SLAP and b) ISP-UNIVE, c) LSCE and d) IGE Internal laboratory isotopicstandards STDs values (%) used for the V-SMOW/SLAP calibration at a) ISP-UNIVE, b) LSCE and c) IGE.</u>

	Standards	δD (‰)	δD uncertainty (‰)	δ ¹⁸ O (‰)	δ ¹⁸ O uncertainty (‰)
a) International	V-SMOV	<u>0</u>	<u>0.5</u>	<u>0</u>	0.02
Standards	SLAP	<u>-428.0</u>	<u>1.0</u>	<u>-55.5</u>	<u>0.10</u>
<u>b</u> a) ISP-UNIVE	TD	-304.9	0.7	-38.36	0.10
	DCS	-407.4	0.7	-51.95	0.10
	AP1	-424.2	0.4	-54.56	0.07
<u>с</u> ь) LSCE	NEEM	-254.1	0.7	-32.89	0.05
	Adelie	-321.0	0.7	-40.55	0.05
	OC4	-422.7	0.7	-53.93	0.05
de) IGE	EGRIP-01	-281.0	0.1	-36.34	0.01

ha formattato: Colore carattere: Automatico

Tabella formattata

GREEN-01	-383.8	0.5	-48.97	0.03
SOUP-01	-388.1	0.1	-49.48	0.01

The CFA-CRDS systems are commonly composed of three main units (Jones et al., 2017a): the ice core-melting component

2.3 CFA-CRDS Coupled System

160

165

175

located in a cold room, which generates continuous stream of liquid water (Fig. 2 - blue block), a vaporiser that converts the liquid into vapor (Fig. 2 - yellow block), and the CRDS isotopic analyser (Fig. 2 - green block). This setup enables online water isotope measurements of δD and $\delta^{18}O$ during the melting of the cores, which are cut in sticks and are loaded vertically above the melt-head (MH). The transport line typically includes a debubbler, which permits the release of air bubbles from the water stream as it passes through, but also promotes additional mixing. A selector valve (SV) prior to the vaporiser allows switching between the CFA line, Ultra Pure Water (UPW) and calibration STDs. The water vapor is transported from the vaporiser to the analyser using a carrier gas (N2 or zero air). The key differences between the three laboratories are summarised in Tab. 2 and Fig. 2. The novel ISP-UNIVE-CFA system is highly scalable according to the specific laboratory needs (Barbaro et al., 2022; Spagnesi et al., 2023). A conductivity device monitors the meltwater stream before it enters the small-volume 200 ul triangular flat cell debubbler. The debubbler has one inlet and two outlets: one for the debubbled meltwater and the other connected to the waste for the air bubbles and excess meltwater, (~0.22 ml min-1). The LSCE-CFA system features a lowdead-volume glass debubbler with a volume of 430 µL, regulated by an automatic flow control to prevent overflow. The system includes a dust filter (A-107 IDEX stainless steel filter, 10 µm size: .189" x .074" x .254") and three conductivity devices. The IGE-CFA system supports a broader range of online analyses and includes a 1,000 μL low-dead-volume glass debubbler. Flow is manually regulated via pump adjustment, and the debubbler is connected to an open line and continuously monitored. Meltwater passes through a 180 µm dust filter and a longer distribution line. The isotopic line includes an additional 20 µm filter and a conductivity device prior to the analyser. The three melt-heads used are similar, featuring a square cross-section with an inner and outer collection area separated by a 2 mm high triangular ridge, as the one described by Bigler et al. (2011). All the three vaporisers are similar and inspired from the capillary-based system described of Gkinis et al. (2010). LSCE and IGE vaporisers were both designed at Paris laboratory, while the ISP-UNIVE one was built at Ca' Foscari University of Venice. The stream is split from the incoming stream into a 50 µm inner diameter fused-silica capillary, and the rest goes into the waste line. The split takes place in a T split with a bore diameter of 0.5 mm. The sample micro-flow is injected in the oven (170°C at ISP-UNIVE and LSCE, and 180°C at IGE), where it vaporises and mixes with dry air or nitrogen, At ISP-UNIVE a mass flow controller (Sensirion AG SFC6000D) is used to control the dry air. The humidity levels at which the continuous analyses are performed are: 10,000-14,000 ppmv, 18,000-22,000 ppmv and 17,000-21,000 ppmv, respectively for ISP-UNIVE, LSCE and IGE. The lower range maintained by ISP-UNIVE represents the maximum level achievable with the nominal setup, balancing melting speed, discrete sample

Formattato: Interlinea: 1,5 righe

ha formattato: Tipo di carattere: Non Corsivo

ha formattato: Non Apice / Pedice

ha formattato: Tipo di carattere: Times New Roman, Cole carattere: Automatico

ha formattato: Tipo di carattere: Times New Roman, Cole carattere: Automatico

ha formattato: Tipo di carattere: Times New Roman, Cole carattere: Automatico, Inglese (Regno Unito)

ha formattato: Tipo di carattere: Times New Roman, Cole carattere: Automatico

ha formattato: Tipo di carattere: Times New Roman, Cole carattere: Automatico, Inglese (Regno Unito)

ha formattato: Tipo di carattere: Times New Roman, Cole carattere: Automatico

ha formattato: Tipo di carattere: Times New Roman, Cole carattere: Automatico, Inglese (Regno Unito) ha formattato: Tipo di carattere: Times New Roman, Cole

carattere: Automatico, Inglese (Regno Unito) ha formattato: Tipo di carattere: Times New Roman, Cole

carattere: Automatico

ha formattato: Tipo di carattere: Times New Roman, Cole carattere: Automatico

ha formattato: Tipo di carattere: Times New Roman, Cole carattere: Automatico

ha formattato: Tipo di carattere: Times New Roman, Cole carattere: Automatico

ha formattato: Tipo di carattere: Times New Roman, Cole carattere: Automatico, Inglese (Regno Unito)

collection via the Fraction Collector, online measurement and the requirement to supply a constant water volume to the CRDS

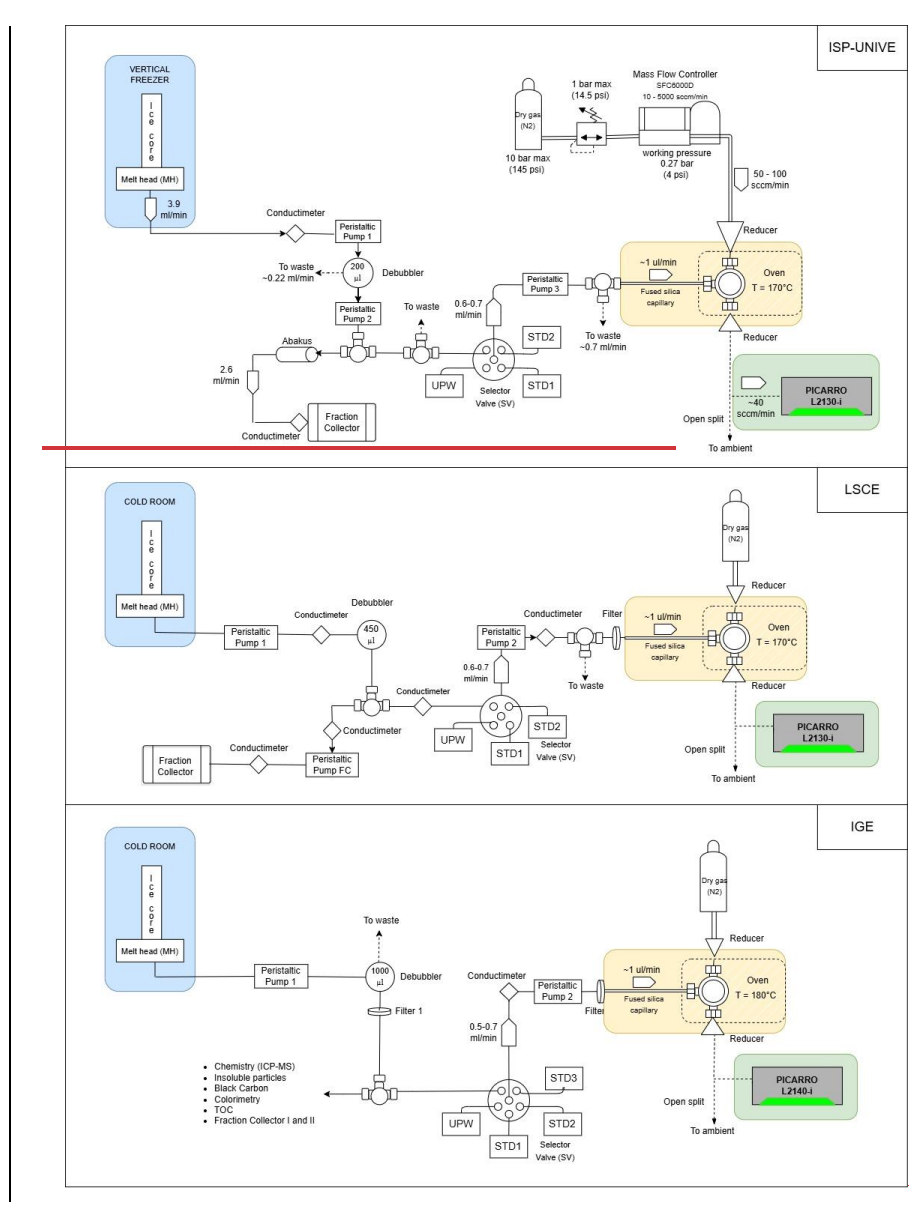
instrument. In general, we do not aim here to isolate the specific impact of each individual system component, as this is beyond the scope of the present study. Rather, we provide a general overview of the factors that may contribute to mixing within the main liquid or vapor phases of the systems. The novel ISP-UNIVE-CFA system (Fig. 2) is highly scalable according to the specific laboratory needs (Barbaro et al., 2022; Spagnesi et al., 2023). The melting unit is located within a vertical freezer. A conductivity device monitors the meltwater stream prior it enters the small volume 200 µl debubbler, which regulates the overflow by continuously discarding part of the flow (-0.22 ml min⁻¹). The isotope line flows through an open T before reaching the vaporiser, possibly promoting ambient air intrusion into the Picarro-L2130 i analyser in case of stick blockage. The vapor mixing ratio is kept between 10,000-14,000 ppmv. The LSCE-CFA system (Appendix A, Fig. A1) is dedicated to continuous isotope measurement and discrete sampling. A 430 µl debubbler is regulated by an automatic flow control to prevent overflow, and the system includes a dust filter (A-107 IDEX stainless steel filter, 10 µm size: 189" x .074" x .254") and three conductivity devices. It keeps vapor mixing ratios between 18,000-22,000 ppmv. The IGE-CFA system (Appendix A, Fig. A2) supports a wider range of online analyses, featuring a 1,000 µl debubbler where the flow is manually regulated by pump adjustment. Meltwater passes through a 180 µm dust filter and a longer distribution line. The isotopic line includes an additional filter (identical to the LSCE one) and a conductivity device prior the analyser, maintaining a humidity levels between 17,000-21,000 ppmv.

180

185

190

ha formattato: Tipo di carattere: Times New Roman, Cole carattere: Automatico



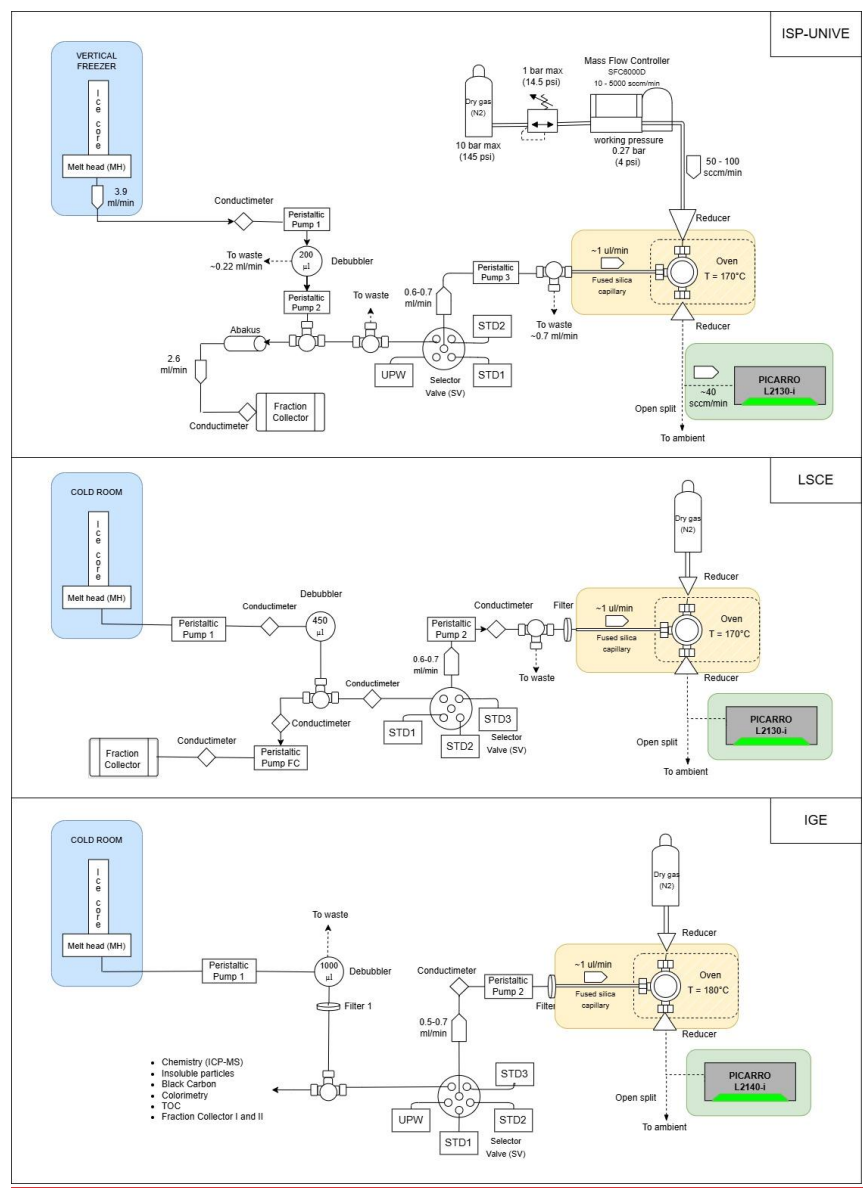


Figure 2. Schematic of the CFA-CRDS systems. The ice core-melting component, the vaporizer and the isotopic analyser are highlighted in blue, yellow and green, respectively. The melting rate is equal to 3 cm min⁻¹.

Table 2. Technical properties for different CFA-CRDS setups

CFA-CRDS setup	ISP-UNIVE	LSCE	IGE
Melt rate (cm min ⁻¹)	3.0±0.5	2.5±0.5	3.0±0.5
Online analysis performed	Water isotopes, insoluble particles	Water isotopes	Water isotopes, ICPMS, insoluble particles, black carbon, TOC and colorimetry
Conductivity devices for isotope line	1	3	1
Pumps for isotope line	3	2	2
Debubbler volume (μl)	200	430	1,000
Filter	No	10 μm filter for the isotopic line	 I) 180 μm filter for the main line II) 10-20 μm filter for the isotopic line
CRDS instrument	Picarro L2130-i	Picarro L2130-i	Picarro L2140-i
Flow rates to the Picarro (ml min ⁻¹)	0.6-0.7	0.6-0.7	0.5-0.7
Humidity (ppmv)	10,000-14,000	18,000-22,000	17,000-21,000

2.4 CFA-CRDS Systems Performance

2.4.1 Impact of the Humidity Level

205

The impact of humidity on the isotopic measurements was evaluated for the three water vapor mixing ratio ranges used during the analyses. The range maintained at ISP-UNIVE, between 10,000 and 14,000 ppmv with occasional fluctuations down to 8,000 ppmv, was assessed using laboratory standard AP1, analyzed in 5 minute intervals at steps of 8,000, 9,500, 11,500, and 14,000 ppmv. For each step, the last 3 minutes were selected. The differences in δ^{18} O and δ D between these humidity levels were smaller than the Allan Deviations (see Sect. 2.4.2) for a 1-second integration time, corresponding at the resolution of the data Picarro output (Fig. 3). For LSCE setup, the same approach was followed with humidity steps performed between 17,000 and 23,000 ppmv. For IGE setup, we relied on above tests confirmed the findings of Gkinis et al., (2010) who validated that variations in δ^{18} O and δ D can be neglected at water vapor mixing ratio in the range 15,000-22,000 ppmv. Consequently, we opted to not apply humidity level correction to the data.

Formattato: SpazioPrima: 0 pt, Dopo: 0 pt, Interlinea: singola

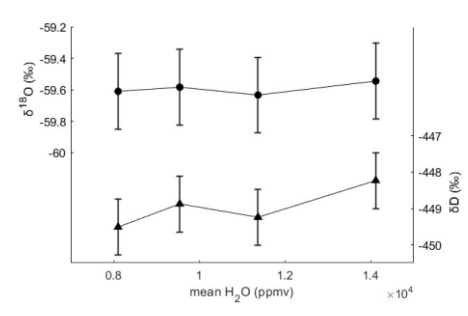


Figure 3: Mean $\delta^{18}O$ and δD values for the 3-minute intervals selected at humidity level of 8,000, 9,500, 11,500 and 14,000 ppmv in the ISP-UNIVE setup. The confidence levels are defined as the Allan Deviation for integration time of 1 s (±1 σ).

2.4.2 Continuous Measurements Noise

210

215

220

225

Measurement noise is quantified using Allan Variance (Allan, 1966) from continuous measurement of a sample of constant isotopic value under humidity conditions that match those CFA-CRDS analyses. Allan Deviation, is an indicator of the stability of the vapor phase signal across varying integration times (τ). The calculation is based on at least 2 hours of UPW flow into the CRDS analyser under stable humidity conditions (Fig. 4, Tab. 3) and thus reflects the stability of the combined vaporiser and CRDS analyser. For the ISP-UNIVE, LSCE, and IGE setups, we select a 1-hour interval with mixing ratios of 14,800±53 ppmv, 20,380±190 ppmv, and 18,100±105 ppmv, respectively. All systems show a decrease with a slope of N⁻¹⁻², characteristic of white noise, for at least τ=250 s, indicating that precision improves with longer integration times. For τ=2 s (corresponding to melting 0.1 cm of ice at 3.0 cm min⁻¹), the SD for δ¹⁸O are 0.17% (ISP UNIVE), 0.15% (LSCE), and 0.06% (IGE). At τ=30 s (time required to melt 1.5 cm of sample), precision improves, with SDs decreasing to 0.05‰, 0.04‰, and 0.02‰, respectively. The IGE system exhibits higher precision, attributed to better instrument performance as indicated by Allan Deviation and the elevated working humidity levels. At ISP UNIVE, the humidity range of 10,000-14,000 ppmv is used despite being outside the instrument's optimum, as large water volumes are required for discrete chemical analysis, and the N₂ flow rate allows for rapid adjustments in case of decreases in the water flow.

Table 3: Allan Deviation for δ^{18} O, δ D and d-excess concerning the integration times (τ) needed to melt 0.1 cm and 1.5 cm of the ice core at the nominal melting rate for each institute.

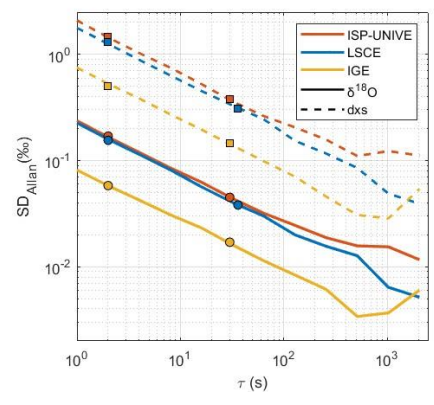


Figure 4: Allan Deviation computed from 1-hour continuous UPW flow for ISP-UNIVE - orange (at 14.850 \pm 53 ppmv), LSCE - blue (at 20.380 \pm 190 ppmv) and IGE - yellow (at 18.100 \pm 105 ppmv) for δ^{48} O and d excess. The dots and squares indicate the specific integration times (τ), for each system, needed to melt 0.1 cm and 1.5 cm of the ice core at the nominal melting rate, respectively.

2.4.3 Mixing in the CFA systems

230

235

240

245

250

The mixing in the CFA system attenuates the original signal preserved in the firn/ice cores, resulting in a smoothing of the isotope record (Gkinis et al., 2011). This effect, analogous to vapor diffusion processes occurring naturally in the firn, arises from the displacement of water molecules from their original relative positions in ice matrix. However, a key distinction between CFA mixing and firm diffusion lies in their respective typical lengths: while firm diffusion typically acts at order of 6-8 cm (Johnsen et al., 2000), mixing is expected to occur over 0.7-1.5 cm (Gkinis et al., 2011; Jones et al., 2017a). Mixing occurs at multiple stages of the CFA setup, including at the melt-head due to water capillarity flow within the porous firn, in the debubbler, within the vaporiser chamber and CRDS cavity, as well as along the transport tubing in both liquid and vapor phase (Jones et al., 2017a)The mixing in the CFA system attenuate the original precipitation signal, smoothing the isotope record (Gkinis et al., 2011). It occur at the melt-head due to water capillarity within the porous firn, in the debubbler, within the vaporiser chamber and the CRDS cavity, as well as throughout the transport tubing in both liquid and vapor phase (Jones et al., 2017a). To assess it, two impulsive responses are quantified using isotopic step functions. In practice, on the one hand, two ice sticks of different isotopic composition are melted in a row to derive the integrated mixing from the melt-head (MH) to evaluate σ_{MH} , and on the other hand, two isotopically distinct liquid samples are introduced at the selector valve (SV) level to determine σ_{SV} . We assess the mixing effect occurring throughout the CFA systems and disentangle the main contributions in the phase upstream and downstream the selector valve. Two different impulse responses are evaluated. The first step function, generated at melt-head stage, (MH), involves the melting of two ice sticks in a row with different isotopic compositions. The second step function includes the mixing downstream the selector valve (SV) by switching between two

ha formattato: Tipo di carattere: Times New Roman, Cole carattere: Automatico

ha formattato: Tipo di carattere: Times New Roman, Cole carattere: Automatico

ha formattato: Colore carattere: Automatico

ha formattato: Colore carattere: Automatico

<u>isotopically distinct liquid samples.</u> The impulse response is determined by fitting a probability density function (PDF) over the first derivative of the Picarro response, described by the normal Gaussian, as suggested by Jones et al., (2017a) (Eq. 1):

1)
$$f(x) = a_1 * exp \left(-\left(\frac{x - b_1}{c_1}\right)^2 \right)$$

where a_1 is the amplitude, b_1 is the mean and c_1 is the standard deviation of the curve. Mixing lengths (σ) are defined as (Eq. 2):

The σ_{MH} reflects the mixing of the entire CFA system, whereas the σ_{SV} represent the mixing downstream the SV. The latter

2)
$$\sigma = \frac{c_1}{\sqrt{2}}$$

260

265

270

280

includes the mixing caused by the presence of a peristaltic pump common to all the three systems and a mixing related to a filter prior the vaporizer for LSCE and IGE (Fig. 2). To estimate mixing length upstream the SV, called σ_L , we calculate the root square of the quadrature difference between σ_{MH} and σ_{SV} (Jones et al., 2017a).

Previous studies used mock ice with varying isotope compositions to calculate σ_{MH} (Dallmayr et al., 2024; Jones et al., 2017a). In this study, we analyse PALEO2 firm core ($\rho = 0.58 \text{ g cm}^{-3}$), which has lower density and higher porosity compared to artificial ice ($\rho = 0.92 \text{ g cm}^{-3}$). Additionally, the mixing in the liquid phase (σ_L) is calculated as the root square of the quadrature difference between σ_{MH} and σ_{SV} (Jones et al., 2017a). To assess the unavailability of Ultra Pure Water (UPW) mock stickss with firn-like density, the σ_{MH} values calculated in this study are based on tests involving different firn/ice transitions. Specifically, a mean value derived from ice-to-ice, ice-to-firn, and firn-to-ice transitions is considered the best laboratory-based approximation of the effective mixing length. We note that the results obtained may differ for deeper and denser ice core sections due to capillary effects. While diffusivity at the melt-head is generally expected to be lower in denser ice due to reduced porosity, the transition from firn to ice is also influenced by changes in melt-head temperature and melt rate, which should be taken into account. However, our

2.5 Data Processing

and then are post-processed. The post-processing includes (i) converting the time to depth scale, (ii) filtering data affected by memory effects and artifacts and (iii) custom block averaged the data at resolution of 0.5 cm.

(i) The depth scale for the isotopic record is built through two common computational steps across all three laboratories. First, the timescale at MH is converted to depth using the measured ice stick lengths and the continuous recording of the encoder position. The encoder (located at the top of the ice sticks) records the melting of the cores at a frequency of ~1 Hz. Second, the arrival time at the CRDS, conductivity cell, and fractionation collectors is calculated based on the peristaltic pump flow rates. At ISP-UNIVE and IGE, the MH-to-CRDS delay is estimated through preliminary tests and corrected for pump rate changes. At LSCE, the MH-to-CRDS time for liquid phase is calculated using the continuously recorded flow rates and the volumes associated with each component of the CFA setup. Additionally, the delay time for gas phase transport to the CRDS

The The isotopic raw data from the Picarro analyser, provided at acquisition time of ~1-s, are calibrated to the V-SMOW/SLAP

ha formattato: Colore carattere: Automatico
ha formattato: Colore carattere: Automatico, Pedice
ha formattato: Colore carattere: Automatico, Pedice
ha formattato: Colore carattere: Automatico, Pedice
ha formattato: Colore carattere: Automatico
Formattato: Interlinea: 1,5 righe
ha formattato: Colore carattere: Automatico
ha formattato: Colore carattere: Automatico, Pedice
ha formattato: Colore carattere: Automatico
ha formattato: Colore carattere: Automatico
ha formattato: Colore carattere: Automatico
ha formattato: Colore carattere: Automatico, Apice
ha formattato: Colore carattere: Automatico

is estimated based on isotopic steps from the SV, under standard operating conditions (specifically, N2 and water flow rates). This gas phase delay is assumed to remain constant throughout the duration of the CFA run. Conductivity profiles plotted on the common depth scale help validated the processing. For LSCE, validation is based on the effective synchronization of three conductivity profiles. At IGE, where a single device is located prior the isotopic analyser, validation relies on aligning conductivity peaks - that correspond to transitions between individual ice sticks - with logged depths. Lastly, adjustments may be required between the actual stick length and the depth logged in the field, particularly for fragile and crumbling firn cores. Temporary blockages or stick collapses can introduce uncertainties when assigning depth to the isotopic profile. Whenever possible, such events should be documented and considered during the interpretation of the depth profiles. (ii) Data at the beginning and end of CFA runs that are affected by mixing with pre- and post-circulated water are manually removed. At ISP-UNIVE, humidity drops - well below the typical work condition - are manually selected using a MATLAB graphical user interface and substituted by linearly interpolated values. (iii) Eventually, data are custom block-averaged at resolution of 0.5 cm. raw data from the Picarro analyser, recorded every second, are post-processed to align isotopic profiles with ice core depth. This includes converting the time scale to depth, calibrating isotopic values to the V-SMOW/SLAP scale, and filtering data affected by memory effects and artifacts. The building of the depth scale for the isotopic record is based on two computational steps common to all three laboratories. First, the timescale at MH is converted into a depth scale of the CFA sticks from the ice sticks' length measured before they are vertically loaded on the ice core-melting component, and from the continuous recording of the encoder position (located at the top of the ice sticks, which records at a frequency of approximately 1 Hz). Second, for each time step at the MH, the corresponding arrival time at the CRDS, conductivity cell, and additional fractionation collectors is calculated based on the flow rates of the peristaltic pumps. For the isotopic record, at ISP-UNIVE, similar to IGE, the delay from MH to CRDS signal recorded is computed through preliminary tests and subsequently corrected for pump rate changes. At LSCE, the arrival time for liquid phase is calculated using the continuously recorded flow rates of the two peristaltic pumps and the volumes associated with each component of the CFA setup. Additionally, the delay time for gas phase transport to the CRDS is estimated based on isotopic steps from the SV, under standard operating conditions (specifically, N2 and water flow rates). This gas phase delay is assumed to remain constant throughout the duration of the CFA run. Conductivity profiles plotted on the common depth scale thus determined allow for validation of the process. For LSCE, which provides three conductivity profiles, validation is achieved through the effective superposition of conductivity features. At IGE, where a single device is used, validation relies on accurately aligning conductivity peaks matching the transitions between individual ice sticks with the logged depths. Lastly, readjustments may be needed between the actual stick length and the depth logged in the field, particularly for crumbling firn cores. Data at the beginning and end of CFA runs that are affected by mixing with pre- and post circulated water are manually removed. For the ISP-UNIVE-CFA results presented in this study, data sections affected by humidity drops lower then ~8,000 ppmv were removed. These intervals were manually selected using a MATLAB graphical user interface, with short gaps (less than 5 minutes, ~ 15 cm depth) interpolated linearly possibly

285

290

295

300

305

310

complications encountered during the initial melting phase, which included firm ice collapse, air bubbles and UPW intrusions resulting from the cleaning process of the tubing during line blockages. No additional data removal was performed in the data series presented for LSCE.

320 2.6 Continuous and Discrete Isotopic Records Comparison Comparison Procedure

The comparison between continuous and discrete isotopic records aims to highlight key technical differences in the CFA-CRDS setups and the operating procedures. Comparisons of profiles versus depth assess the agreement in calibration and depth scale attribution between laboratories. Additionally, the power spectral density (PSD) analysis - defined as the measure of signal's power content in the frequency domain - reveals system limitations caused by mixing and measurement noise. Before presenting the comparison in Sect. 3, we briefly introduce the PSD approach (Fig. 3), providing an idea of the mixing and measurement noise effects in the continuously measured signal. For this purpose, we consider ideally the discrete record as the best available approximation of the true signal preserved in the ice, limited only by discrete sampling resolution and uncertainties in the depth for sampling cut. The discrete spectrum shows a "flat" shape at frequencies around 100 m. (white area), where the signal is dominated by precipitation intermittency and stratigraphic noise The comparison between continuous and discrete isotopic records aims to highlight key technical differences in the CFA-CRDS setups and the operating procedures. Comparisons of profiles versus depth assess the agreement in calibration and depth scale attribution between laboratories, while the power spectral density (PSD) analysis defined as the measure of signal's power content in the frequency domain reveals system limitations caused by mixing and measurement noise. Before detailing the comparison in Sect. 3, we briefly describe the PSD approach (Fig. 5). Here, the discrete record is ideally considered as the best approximation of the true signal preserved in the ice, limited only by discrete resolution and uncertainties in the depth for sampling cut. Since its spectrum lacks a flat region typically indicative of white noise - at high frequencies, measurement noise never dominates over the signal. The discrete spectrum is flat at frequencies around 1 m⁻¹ (white area), dominated by precipitation intermittency and stratigraphic noise (Casado et al., 2020; Laepple et al., 2018). This is because, at these frequencies, the observed variability arises from random processes rather than from climatic trends or seasonal signals. In contrast, attenuation begins at 50 cm⁻¹ (yellow area), consistent with diffusion effects (Johnsen et al., 2000). For the 12-16 m depth section of cores collected on the Antarctic plateau, such as the PALEO2 core (density of ~0.58 g cm⁻³), firn diffusion is estimated by previous studies to have a length of 6-8 cm for δ^{18} O In contrast, it attenuates for scales between 0.5-0.9 m⁻¹ (yellow area), corresponding to diffusion (Johnsen et al., 2000). This firm diffusion, with length of 10-15 cm (Gkinis et al., 2021; Johnsen et al., 2000; Lacpple et al., 2018; Whillans & Grootes, 1985). Diffusion effect can be modelled by the following Eq. 3, can be modelled by Eq. (1) (Johnsen et al., 2000):

$$P = P_o \exp(-k^2 \sigma_{diff}^2)$$

325

330

335

where σ_{diff} represents the firn diffusion length, and k=2 π f, with f being the frequency.

ha formattato: Apice

ha formattato: Colore carattere: Automatico

ha formattato: Tipo di carattere: (Predefinito) Cambria M ha formattato: Tipo di carattere: (Predefinito) Cambria M ha formattato: Tipo di carattere: (Predefinito) Cambris M

ha formattato: Tipo di carattere: (Predefinito) Cambria M ha formattato: Tipo di carattere: (Predefinito) Cambria M

ha formattato: Tipo di carattere: (Predefinito) Cambria M

ha formattato: Tipo di carattere: (Predefinito) Cambria M ha formattato: Tipo di carattere: (Predefinito) Cambria M

ha formattato: Tipo di carattere: (Predefinito) Cambria M

ha formattato: Tipo di carattere: (Predefinito) Cambria M

ha formattato: Tipo di carattere: (Predefinito) Cambria M Formattato: Giustificato, Rientro: Prima riga: 1,27 cm,

SpazioPrima: 12 pt, Dopo: 12 pt

At higher frequencies (\sim 3-20 cm⁻¹), a signal power is still observed. This noise likely arises in parallel with or after diffusion processes, and can be probably related to stratigraphic or other post-depositional processes. Indeed, we note that this spectral feature is preserved in both discrete and CFA records, and it appears attenuated in the latter due to signal mixing. However, the origin mechanism of this spectral power remains unclear and a comprehensive investigation of this phenomenon lies beyond the scope of the present study. Here, we aim to use the discrete dataset - resampled at 0.5 cm resolution to match the post-processed resolution of the continuous record - as a reference signal to which mixing and measurement noise are applied. To this end, we apply an Mixing in the CFA behaves similarly to diffusion, albeit on a much smaller scale around 0.7-1.5 cm (Gkinis et al., 2011; Jones et al., 2017a). We theoretically simulate the continuous spectrum from the discrete one, by applying additional Gaussian smoothing to account for the CFA mixing length (σ_{mix}) and incorporating the measurement noise (ε_N) determined for the online analysis, as described by the following equation (Eq. 4)Eq. (2):

4)
$$P = P_4 \exp(-k^2 \sigma_{mix}^2) + \varepsilon_N$$

As a result, The simulated spectrum diverges from the discrete spectrum at the frequency where CFA mixing begins to affect the signal, showing smoothing in the medium frequency range (>0.5 m⁻¹, orange area) and flattering at higher frequencies due to measurement noise (brown area). Measurement noise generates a flat spectrum at the frequency where the Signal-to-Noise Ratio (SNR) equals 1 (Casado et al., 2020), permitting to determine the frequency limit where meaningful climatic information can still be retrieved as the point where the spectra of signal and noise intersect. Beyond this limit, noise dominates the signal, as the correlation between the record and the signal is defined as (Eq. 5):

$$365 5) r^2 = \frac{SNR}{1+SNR}$$

350

355

At SNR = 1, a minimum significant correlation $r = \sqrt{0.5} \sim 0.71$ is reached. A similar behaviour is expected for the power spectral densities (PSDs) of the continuous records, allowing us to identify the maximum reliable frequency retained in the signal.

ha formattato: Colore carattere: Automatico

ha formattato: Tipo di carattere: (Predefinito) Cambria №
ha formattato: Tipo di carattere: (Predefinito) Cambria №
ha formattato: Tipo di carattere: (Predefinito) Cambria №

ha formattato: Tipo di carattere: (Predefinito) Cambria M ha formattato: Tipo di carattere: (Predefinito) Cambria M

ha formattato: Tipo di carattere: (Predefinito) Cambria M

ha formattato: Tipo di carattere: (Predefinito) Cambria M **ha formattato:** Tipo di carattere: (Predefinito) Cambria M

ha formattato: Tipo di carattere: (Predefinito) Cambria M

ha formattato: Tipo di carattere: (Predefinito) Cambria M

ha formattato: Tipo di carattere: (Predefinito) Cambria M ha formattato: Tipo di carattere: (Predefinito) Cambria M

ha formattato: Tipo di carattere: (Predefinito) Cambria M

ha formattato: Tipo di carattere: (Predefinito) Cambria M Formattato: Rientro: Prima riga: 1,27 cm, SpazioPrima:

pt, Dopo: 12 pt

Formattato: SpazioPrima: 12 pt, Dopo: 12 pt

ha formattato: Colore carattere: Automatico

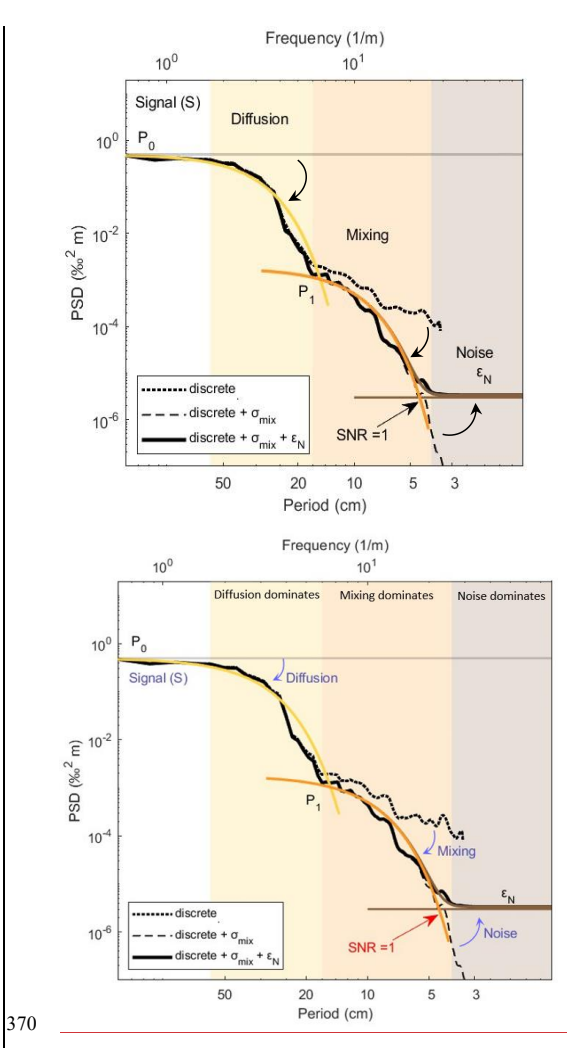


Figure 53. Schematic PSD of discrete and simulated profiles. The simulated spectrum (solid black line) is obtained by combining the discrete power density (dashed black line) affected by natural diffusion in the firn (σ_{diff} – yellow) with the mixing effect occurring in the CFA system (σ_{mix} – orange) and the measurement noise associated with continuous measurements (ε_N – brown).

3 Results

390

395

375 In this section, we compare the measurements of the same 4-m section of the PALEO2 firm core by the CFA setups of ISP-UNIVE, LSCE, and IGE with the discrete results. By analysing both in the depth and in spectral domains, we evaluate the precision and accuracy of each setup and operational procedure. In turn, we assess the effective resolution limit at which a reliable isotopic signal can be retrieved from the CFA outputs, based on each system's internal mixing and measurement noise.

32.4.1 Continuous Measurements Noise

To assess the stability and noise of the combined vaporiser and CRDS analyser, we calculate the Allan Variance (Allan, 1966) on isotopic time series (example of ISP-UNIVE time series is presented in Appendix B_s. Fig. B₁). The time series are continuous measurement of UPW under constant humidity conditions that match those of CFA-CRDS analyses. The Allan Variance is computed taking a time series of size N. The data are divided into m non-overlapping intervals, each containing k=N/m data points. The acquisition time per data point is fig. then the integration time for each interval is \(\pi_{m_0} = k f_{in} \). The Allan Variance for a given \(f_{m_0} = k f_{in} \) is defined as (Eq. 6).

6)
$$\sigma^2(\tau_m) = \frac{1}{2m} \sum_{j=1}^m \left(\bar{\delta}_{j+1} - \bar{\delta}_j\right)^2$$

where $\bar{\delta}_{j+1}$ and $\bar{\delta}_{j}$ are the mean values of neighbouring non-overlapping intervals j and j+1. This method quantifies the timedependent variance between consecutive intervals, making it particularly suitable for evaluating noise and drift in highresolution continuous measurements. Measurement noise is quantified using Allan Variance (Allan, 1966) from continuous measurement of a sample of constant isotopic value under humidity conditions that match those CFA-CRDS analyses. Allan Deviation, is an indicator of the stability of the vapor phase signal across varying integration times (τ). The calculation is based on at least 2 hours of UPW flow into the CRDS analyser under stable humidity conditions (Fig. 4, Tab. 3) and thus reflects the stability of the combined vaporiser and CRDS analyser. For the ISP-UNIVE, LSCE, and IGE setups, we select a 1-hour interval with mixing ratios of 14,800±53 ppmv, 20,380±190 ppmv, and 18,100±105 ppmv, respectively. The calculation is based on continuous UPW flow into the CRDS analyser under stable humidity conditions (Fig. 4, Tab. 3). For ISP-UNIVE, LSCE, and IGE, the mixing ratios are ~14,800 ppmv, ~20,000 ppmv, and ~18,100 ppmv, respectively. For ISP-UNIVE and LSCE we selected 2-hour of continuous data, while for IGE 1.5-hour time series was used. The raw data, provided each 0.85s for L2130i models (ISP-UNIVE and LSCE) and each 0.72s for L2140-i model (IGE), are interpolated at 1-s post-acquisition. All systems show a decrease with a slope of $N^{-1/2}$, characteristic of white noise, for at least τ =250 s, indicating that precision improves with longer integration times. For $\tau=2$ s (corresponding to melting 0.1 cm of ice at 3.0 cm min⁻¹), the SD for δ^{18} O are 0.17 ‰ (ISP-UNIVE), 0.15 ‰ (LSCE), and 0.06 ‰ (IGE). At τ=30 s (time required to melt 1.5 cm of sample), precision improves, with SDs decreasing to 0.05 %, 0.04 %, and 0.02 %, respectively. **Picarro L2140-i analyser used at IGE demonstrates higher precision than the L2130-i model used at LSCE, despite operating at lower humidity levels during the Allan variance

ha formattato: Colore carattere: Automatico

Formattato: Interlinea: 1,5 righe
ha formattato
ha formattato
ha formattato
ha formattato
ha formattato
ha formattato
Formattato: Rientro: Prima riga: 1,27 cm, SpazioDopo: pt, Interlinea: 1,5 righe
ha formattato: Tipo di carattere: 10 pt, Colore carattere: Automatico
ha formattato
ha formattato

ha formattato: Colore carattere: Automatico

assessment. In addition, the L2130-i analyser at ISP-UNIVE shows a precision comparable to that at LSCE, even though
measurements were also conducted at lower humidity. These results suggest that precision and instrument noise are primarily
determined by the analyser's intrinsic performance rather than the specific technical configuration of the CFA system.

However, due to the considerable variability among Picarro instruments, a detailed explanation for the better performance of
the L2140-i relative to the L2130-i lies beyond the scope of this study.he IGE system exhibits higher precision, attributed to
better instrument performance as indicated by Allan Deviation and the elevated working humidity levels. At ISP-UNIVE, the
humidity range of 10,000-14,000 ppmv is used despite being outside the instrument's optimum, as large water volumes are
required for discrete chemical analysis, and the N2 flow rate allows for rapid adjustments in case of decreases in the water
flow.

<u>Table 3. Allan Variance for $\delta^{18}O$, δD and d-excess concerning the integration times (τ) needed to melt 0.1 cm and 1.5 cm of the ice core at the nominal melting rate for each institute.</u>

	Melt rate	SD 0.1 cm			<u>SD_1.5 cm</u>			
	(cm min ⁻¹)	<u>δ¹⁸O (‰)</u>	<u>δD (‰)</u>	<u>dxs</u> (‰)	<u>δ¹8O (‰)</u>	<u>δD (‰)</u>	$\underline{\mathbf{d}_{xs}}$ (‰)	
ISP-UNIVE	3.0	0.17	0.55	1.47	0.05	0.16	0.38	
LSCE	<u>2.5</u>	0.15	0.26	1.30	0.04	0.07	0.31	
<u>IGE</u>	3.0	0.06	0.20	0.60	0.02	0.06	0.14	

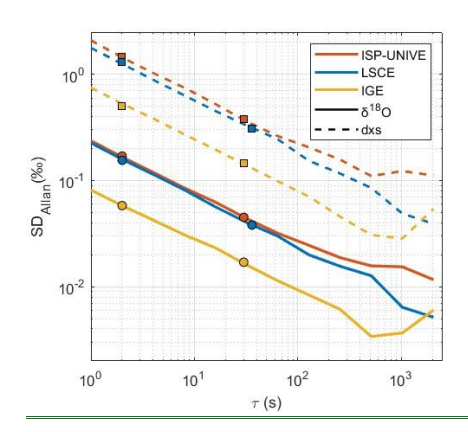


Figure 44. <u>Allan Variance computed from 1-hour continuous UPW flow for ISP-UNIVE - orange (at 14.850 \pm 53 ppmv), LSCE - blue (at 20.380 \pm 190 ppmv) and IGE - yellow (at 18.100 \pm 105 ppmv) for δ^{18} O and d-excess. The dots and squares indicate the specific integration times (τ), for each system, needed to melt 0.1 cm and 1.5 cm of the ice core at the nominal melting rate, respectively.</u>

420 32.4.2 Impact of the Humidity Level

The impact of humidity on the isotopic measurements was evaluated for the three water vapor mixing ratio ranges used during the analyses. The range maintained at ISP-UNIVE, between 10,000 and 14,000 ppmv with occasional fluctuations down to 8,000 ppmv, was assessed using laboratory standard AP1, analysed in 5-minute intervals at steps of 8,000, 9,500, 11,500, and 14,000 ppmv. For each step, the last 3 minutes were selected. The differences in δ^{18} O and δ D between these humidity levels were smaller than the Allan Variance (see Sect. 2.43₂1) for a 1-second integration time, corresponding at the resolution of the data Picarro output (Fig. 53). For LSCE setup, the same approach was followed with humidity steps performed between 17,000 and 23,000 ppmv. For IGE setup, we relied on above tests confirmed the findings of Gkinis et al., (2010) who validated that variations in δ^{18} O and δ D can be neglected at water vapor mixing ratio in the range 15,000-22,000 ppmv. Consequently, we opted to not apply humidity level correction to the data.

430 Between 10,000 and 20,000 ppmv, the precision of the Picarro instrument at time scales comparable to those of the CFA remains relatively stable. This was assessed through an Allan Variance analysis conducted across humidity levels in the 10,000–20,000 ppmv range (see Appendix A, Fig. A1, Tab. A1).

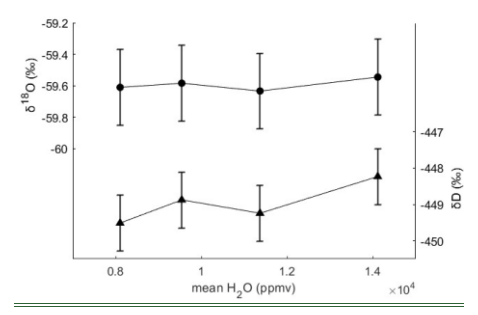


Figure 35. Mean δ^{18} O and δ D values for the 3-minute intervals selected at humidity level of 8,000, 9,500, 11,500 and 14,000 ppmv in the ISP-UNIVE setup. The confidence levels are defined as the Allan Variation for integration time of 1 s ($\pm 1\sigma$).

3.31 Evaluation of Mixing Lengths from Impulse Response Mixing Lengths

The Here, we present the mixing lengths of the three systems, evaluated from melt-head stage (MH), which reflects the total mixing within the CFA-CRDS systems, and from the selector valve stage (SV). The theoretical basis for these calculations is detailed in Section 2.4.

Due to the unavailability of a UPW mock stick with firn-like density, we tested different transition types: ice-to-firn, firn-to-ice, and ice-to-ice (Appendix C, Tab. C1). Although the mixing lengths may vary depending on the density of the sticks during

underestimated for firn-to-firn case. Figure 6a show an example of a normalised step function: firn-to-ice transitions are shown for ISP-UNIVE and LSCE, while an ice-to-firn transition is shown for IGE. Prior to normalization, the isotopic difference between ice sticks at MH (or liquid standards at SV) ranges from 40-50 % for δ^{18} O and 380-400 % for δ D. The corresponding impulse responses are presented in Figure 6b. The mixing lengths from MH derived for each laboratory show no significant differences across transition types (Tab. B1). We therefore define own as the mean value of all transitions, which will 450 correspond to σ_{mix} in the back-diffusion approach presented in the following sections. The mixing lengths (σ_{MH} , σ_{SV} and σ_L) are summarized in Table 4. Since the values for $\delta^{18}O$ and δD are very similar, we report only $\delta^{18}O$. The resulting mean σ_{MH} values are 7.1 mm for LSCE, 11.3 mm for ISP-UNIVE, and 18.2 mm for IGE. quantified mixing lengths for the three inspected systems are based on step functions at level of the melt-head (σ_{MH}), correspondent to the total mixing in the systems (defined as σ_{mix} in the other Sections), and at level of the selector valve (σ_{SX}) as shown in Fig. 455 6 and Tab. 4. Previous studies used mock ice with varying isotope compositions to calculate σ_{MH} (Dallmayr et al., 2024; Jones et al., 2017a). In this work, the PALEO2 firn core ($\rho = 0.58 \text{ g cm}^{-3}$) has a lower density and higher porosity than the artificial $ice (\rho = 0.92 \text{ g cm}^3)$, potentially leading to an underestimation of the mixing lengths when quantified based on ice to ice transitions. We compared the mixing lengths obtained from ice to-firn, firn to-ice, and ice to-ice transitions (Appendix B, Tab. B1), determining no significant differences in capillary action. Therefore, we used the mean value as the σ_{mix} in our back-460 diffusion approach, and discuss the potential difference with the more realistic case of firm to firm transitions (see Discussion). The differences in isotopic composition between firn and mock UPW-ice are 40-50% for δ ¹⁸O and 380-400% for δ D. The mixing lengths for δ^{18} O and δD are very similar, so we present the results for δ^{18} O. The mean σ_{MH} values are 7.1 mm for LSCE. 11.3 mm for ISP UNIVE, and 18.2 mm for IGE (Tab. 4). The mixing length in the liquid phase (σ_t) is calculated as the root square of the difference in quadrature between σ_{MH} and σ_{SV} . Values expressed in seconds are converted in millimeters, using 465 the average melting rate. Overall, LSCE system exhibits the smaller σ_{MH} , indicating the most efficient setup among the three systems evaluated. In contrast, IGE-CFA shows the highest σ_{MH} (Tab. B1), with the dominant contribution arising from mixing in the liquid phase, as reflected by the higher σ_L . This is likely due to the presence of a high-volume debubbler and a longer distribution line, required to accommodate the higher number of online measurements and discrete sampling operations performed by the laboratory. Notably, ISP-UNIVE shows more diffusion downstream of the selection valve (20.0s) than upstream (10.1s). This behaviour contrasts with the other systems presented in Tab. 4, including values for ice-to-ice transitions previously reported by Jones et al. (2017a) at the Institute of Arctic and Alpine Research (INSTAAR) Stable Isotope Lab (SIL) and by Dallmayr et al. (2024) at the Alfred-Wegener-Institut Helmholtz-Zentrum für Polar-und Meeresforschung (AWI). This higher σ_{SV} observed in the ISP-UNIVE system is presumably attributed to the presence of a T-split before the vaporiser, which likely increases mixing. In addition, the relatively low σ_L may result from the compact configuration of the system, there the melting

melting, this approach provides the best estimate within the given experimental constraints, even if the values may be slightly

ha formattato: Tipo di carattere: Corsivo
ha formattato: Tipo di carattere: Corsivo
ha formattato: Pedice
ha formattato: Pipo di carattere: Corsivo
ha formattato: Tipo di carattere: Corsivo
ha formattato: Tipo di carattere: Corsivo
ha formattato: Tipo di carattere: Corsivo
ha formattato: Pedice

ha formattato: Colore carattere: Automatico

ha formattato: Colore carattere: Automatico

unit is in a vertical freezer near the instruments, unlike located in cold rooms with longer distribution lines.

LSCE exhibits the smaller σ_{AHI} attributed to its shorter distribution line and the more efficient isotopic analysis setup. Conversely, IGE-CFA has the highest σ_{AHI} (Tab. B1) reflecting the higher volume debubbler and the longer distribution line. Notably, IGE exhibits a higher σ_{SV} compared to LSCE, despite showing a lower Allan variance, which reflects the performance of the combined vaporiser-Picarro system.

The mixing lengths are consistent with the values reported by Jones et al. (2017a) at the Institute of Arctic and Alpine Research (INSTAAR) Stable Isotope Lab (SIL) and by Dallmayr et al. (2024) at the Alfred-Wegener-Institut Helmholtz-Zentrum für Polar-und Meeresforschung (AWI) for ice-to-ice transitions, equal to 7 mm and 13.6 mm, respectively (Tab. 4).

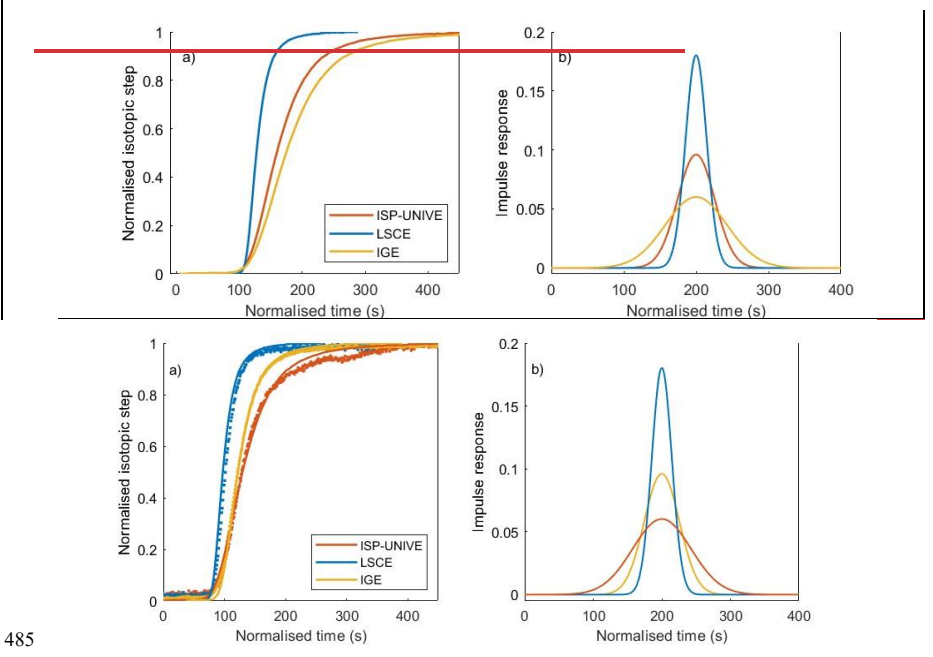


Figure 6. a) Raw data interpolated at 1-s post-acquisition and respective normalised transfer function for ice steps at stage of the CFA melt-head for δ^{18} O. b) Normal PDF impulse response function. Firn-to-ice transitions are shown for ISP-UNIVE and LSCE, while an ice-to-firn transition is shown for IGE. Figure 6: a) The normalised transfer function and b) the normal PDF impulse response function for ice steps at level of the CFA melt-head for δ^{18} O.

Table 4: δ¹⁸O mixing lengths at melt-head level stage (σ_{MH}) and at selector-valve level stage (σ_{SV}) for the three different CFA-CRDS systems. The mixing length in the liquid phase (σ_L) is calculated as the difference in quadrature of σ_{MH} and σ_{SV}. The mixing length expressed in seconds is converted in millimeters considering the average melting rate set at the three institutes. The ISD are given in parenthesis. The mixing lengths are compared with Jones et al., 2017a at the Institute of Arctic and Alpine Research (INSTAAR) Stable Isotope Lab (SIL) and Dallmayr et al., 2024 at the Alfred-Wegener-Institut Helmholtz-Zentrum für Polar-und Meeresforschung (AWI).

System	Melt rate	омн (s)	σ _{MH} (mm)	σsv (s)	$\sigma_L(s) \sigma_L(mm)$

(cm	min-1
(CIII	111111

	ISP-UNIVE	3	22.4 (2.0)	11.2 (1.0)	20.0 (0.6)	10.1	5.1
This work	LSCE	2.5	16.8 (2.2)	7.1 (0.9)	8.6 (1.4)	14.4	6
	IGE	3	36.4 (6.0)	18.2 (3.0)	16.8 (2.3)	32.3	16.2
From literature	INSTAAR	2.5	17.4 (2.2)	7 (0.9)	9.4 (0.5)	14.6	6
	AWI	3.8	21.6 (2.4)	13.6 (1.5)	12.6 (1.8)		4.5

3.42 Discrete vs Continuous Data

505

We present the continuous δ^{18} O and *d-excess* records from ISP-UNIVE, LSCE and IGE in comparison with the discrete profiles (Fig. 7). For both ISP-UNIVE and IGE, the top 0.50 m of the first bag was removed due to complications encountered during the initial melting phase of the firn cores. These issues were related to the collapse of firn sticks at the melt head and the intrusion of particles into the distribution line, which required cleaning with UPW. As a result, we show the PALEO2 data from the 12.5-16 m depth section. The CFA data, provided at 0.5 cm resolution after post-processing, was block-averaged at lower resolution by matching the discrete depth intervals (Fig. 7. a and c; original data in Appendix D, Fig. D1).

A representative example regarding the X-axis values (melt rates and their associated standard deviation) prior the conversion in depth are provided in Appendix E, Fig. E1. The differences between the averaged continuous and discrete data are analysed using histograms of the differences at each depth point (Fig. 7. e and f), and statistical significance is assessed using a Kruskal-Wallis non-parametric ANOVA test. Differences with $p \le 0.05$ are considered statistically significant. Overall, the variability in ice core £18O records, primarily at the decimetric scale, is comparable between the three CFA profiles and the discrete sampling, showing no statistically difference. In detail, the ISP-UNIVE-CFA shows difference of -0.01±0.26 ‰ (mean ± 1σ). 510 Two data sections exhibit larger differences to the discrete profile, corresponding to depths of 13.85-13.96 m and 15.62-15.85 m (Fig. 7a, orange areas). The first interval involves ~15 cm of data removed and interpolated due to a humidity drop to 1,200 ppmv. The second interval shows a humidity fluctuation to 7,850 ppmv, slightly below the typical working conditions. This section has been retained. For the LSCE-CFA, the mean difference for $\rho_{\rm L}^{\rm ISO}$ is slightly higher but remains non-significant, with a SD within the instrument's error (0.13 \pm 0.18 % for δ ¹⁸O, Tab. 5). The IGE-CFA results show a difference of -0.06 \pm 0.24 % compared to the discrete data. The SD, similar to that of ISP-UNIVE but larger than that of LSCE, is primarily attributed to small depth scale shifts (Fig. 7b). For d-excess, the ISP-UNIVE and IGE show statistically difference from the discrete data of -0.78±0.64 ‰ and 0.88±0.48 ‰, respectively. These discrepancies are mostly attributed to calibration, as shown by the reduced difference after applying a calibration correction that aligns the mean difference to zero (Fig. 7d). In contrast, the LSCE record shows a non-significant difference of 0.03±0.55 %.

520 Overall, the good agreement between CFA and discrete record for both £18O and d-excess suggests that the LSCE data processing is the most reliable among the three CFA setups, which is why the entire PALEO2 core was analysed at LSCE (Sect. 4). The CFA data, initially provided at 0.5 cm resolution after post-processing, have been integrated at the lower ha formattato: Tipo di carattere: Corsivo

ha formattato: Colore carattere: Automatico

ha formattato: Colore carattere: Automatico ha formattato: Colore carattere: Automatico

ha formattato: Tipo di carattere: Corsivo ha formattato: Apice

ha formattato: Tipo di carattere: Corsivo ha formattato: Apice

ha formattato: Tipo di carattere: Corsivo ha formattato: Apice

resolution that matches the discrete depth intervals to highlight the main differences (Fig. 7. a and e; the original data are presented in Appendix C. Fig. C1). The differences between the averaged continuous and discrete data are analysed using histograms of the differences at each depth point (Fig. 7, e and f). Overall, the variability in ice core δ¹⁸O records, primarily at the decimetric scale, is comparable between the three CFA profiles and the discrete sampling, showing no statistically difference. The ISP-UNIVE-CFA results have no significant difference of $-0.01\pm0.26\%$ (mean \pm 1σ) for δ^{HS} O. However, two sections - showing higher difference with discrete profile - were not removed during data post-processing. These intervals correspond to depths of 13.85-13.96 m and 15.62-15.85 m (Fig. 7a, orange areas). The first was caused by a humidity drop to 1,200 ppmv, where the isotopic record was removed and linearly interpolated. The second interval consisted in a humidity drop to 7,850 ppmv, slightly below the limit of water vapor mixing ratio imposed during typical analysis campaign, which was retained to highlight the impact of humidity fluctuation. Although rare, such events occurred in the novel coupling of the CFA-CRDS at ISP-UNIVE, where achieving a highly consistent flow rate was challenging during initial analysis. For the LSCE-CFA, the mean difference for δ^{48} O is slightly higher but remains non-significant, with a SD within the instrument's error (0.13±0.18% for δ^{48} O, Tab. 5). The IGE-CFA results compared with discrete data show difference of -0.06±0.24% for δ^{48} O. The SD, comparable to that of ISP-UNIVE but larger than that of LSCE, is primarily attributed to small shifts in the depth scale. These centimeter-scale shifts are evident near the transitions between peaks (Fig. 7b). For d-excess, the ISP-UNIVE and IGE results show statistically difference with discrete data of -0.78±0.64% and 0.88±0.48%, respectively. These discrepancies are mainly attributed to calibration, as supported by the reduced difference between discrete and CFA data after applying a ealibration correction that shifts isotopic values to align the mean difference to zero (Fig. 7d). By contrast, the LSCE record show a non-significant difference of $0.03\pm0.55\%$. Overall, the good agreement in both $\delta^{18}O$ and d-excess between CFA and discrete records indicates that the LSCE calibration process is the most robust among the three CFA setups for this series, which is why the entire PLAEO2 core was analysed at LSCE (Sect. 4).

525

530

535

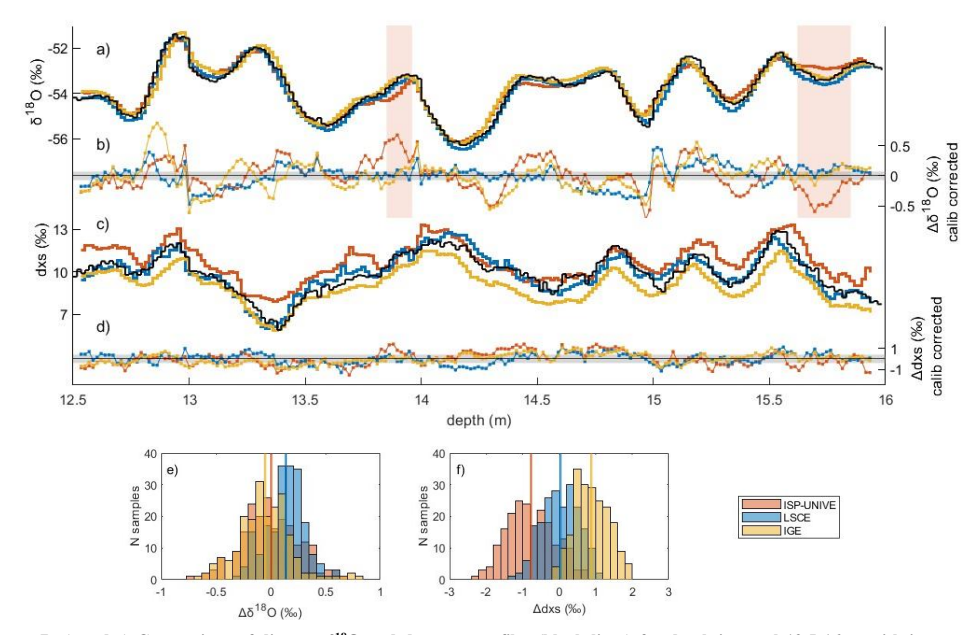


Figure 7. a) and c) Comparison of discrete $\delta^{18}O$ and d-excess profiles (black lines) for depth interval 12.5-16 m with integrated discrete record built from CFA measurements for ISP-UNIVE (orange), LSCE (blue) and IGE (yellow). The histograms e) and f) represent the distribution of difference between discrete data and discrete record built from CFA measurements. b) and d) show the difference between discrete data and discrete record built from CFA measurements corrected for calibration. The horizontal grey areas represent the uncertainties of the discrete analysis for $\delta^{18}O$ and d-excess.

Table 5. Mean, SD and Root Mean Square (RMS) of the isotope difference between discrete and CFA data for ISP-UNIVE, LSCE and IGE. Significant differences (p < 0.05 using a Kruskall-Wallis nonparametric ANOVA test) are represented as bold.

		λδ ¹⁸ O (‰)	Δd_{xs} (‰)			
	Mean	SD	RMS	Mean	SD	RMS	
ISP-UNIVE	-0.01	0.26	0.26	-0.78	0.64	1.00	
LSCE	0.13	0.18	0.22	0.03	0.55	0.55	
IGE	-0.06	0.24	0.25	0.88	0.48	1.00	

3.53 Impact of Diffusion and Mixing on the Signal Spectral Analysis

545

555

In this section, we conduct a PSD analysis on continuous and discrete results (Fig. 8) to assess the impact of mixing on continuous measurements and to determine the frequency limit at which the measurement noise begins to dominate over the

signal. The continuous data has a post-processed resolution of 0.5 cm, while the discrete samples have a resolution of 1.7 cm. Diffusion, with a length of 6-8 cm in firn, begins to smooth the climatic signal at periods around 50 cm (as observed in the yellow areas of Fig. 8). In the range 20-50 cm (yellow area), diffusion emerges as the dominant process shaping the spectra. At smaller scales (3-20 cm – orange area), however, additional mixing, characterised by mixing lengths of a few centimetres, further attenuates the power preserved in the discrete spectrum. This power is not only associated with instrumental noise but may be attributed to additional post-depositional processes occurring in parallel with or after diffusion, which will not be investigated in this study. 10-15 cm in firn, primarily smooths the climatic signal over period of 20-50 cm (yellow areas). Conversely, mixing within the CFA systems, characterised by lengths of a few centimeters, further attenuates the continuous signal over periods of 3-20 cm, as shown by the discrepancies between CFA and discrete spectra (orange areas).

560

lines S) and the noise flat spectrum (brown areas, black dashed lines ϵ_N), where the SNR equals to 1. These resolution limits are 1.8 cm for ISP-UNIVE, 1.6 cm for LSCE, and 1.3 cm for IGE. While the effects of mixing can be corrected by applying back-diffusion to the signal, attempting this on frequencies dominated by measurement noise would result in an artificial amplification of that noise. However, as the primary objective of this study is to provide a straightforward approach for determining the resolution at which measurement noise begins to dominate the signal, the records will be custom-block averaged at that determined resolution. This process effectively removes measurement noise, additionally removing the amplification of noise that could result from back-diffusion process.

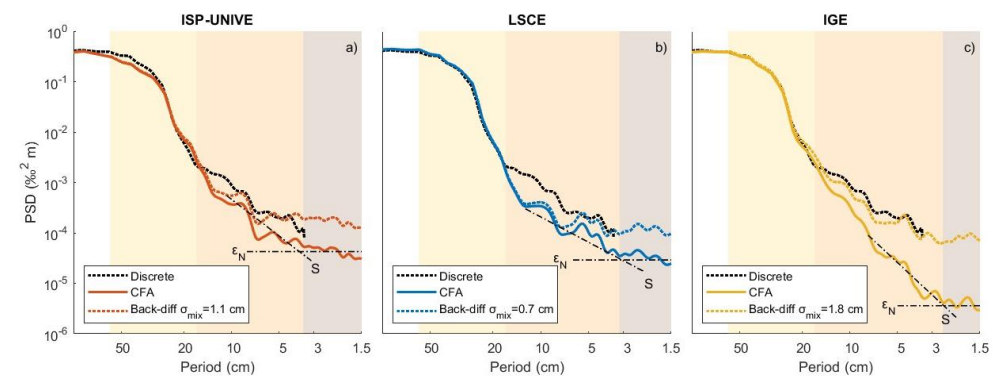
The frequency limit for reliable isotopic measurements corresponds to the intersection of the smoothed signal (black dashed

The filter used for deconvolving the mixing effect in isotopic time series, applies a back-diffusion method using a Gaussian 575 kernel-based approach. Taking the time series and the nominal σ_{mix} (Sect. 3.3) as input, for each data point in the time series, a Gaussian kernel is constructed based on the mixing length. The kernel is centred on the current point and extended to the surrounding points, with the width of the kernel determined by the diffusion length. The kernel is then normalized, and the values within the kernel range are weighted and convolved with the original data to produce a diffused value for each point. This smoothing process captures the effects of diffusion generating an artificial diffused record. Then, the inverse Fourier 580 transform is calculated on the difference between original and diffused signals and is applied to the original signal to restore the higher frequencies. Back diffusion applies an inverse Fourier transform, generated based on the nominal σ_{mix} (Sect. 3.1), to the original record restoring the power of the higher frequencies. The back-diffused profiles show significant improvement in the amount of signal across the 3-10 cm period range for all three CFA systems. The lack of signal for periods ranging from 10 to 20 cm in the LSCE profile, and to some extent in the ISP-UNIVE, is not corrected by this back-diffusion, which does not act at such frequencies. However, although we observe a correction of the high frequencies in the spectral domain, this adjustment proves to be negligible when comparing the back-diffused data with discrete samples along the depth scale (Appendix FE, Fig. FE1). This is because the signal is dominated by low frequencies -with approximately 1000 times more power at the 50 cm scale than at the 10 cm scale - and the restored high-frequency power remains relatively weak. Overall, as the signal is dominated by the lower frequency (1000 times more power at the 50 cm seale than at the 10 cm seale), this does not affect the performances of the comparison between the CFA setups and the discrete time series, as shown for the backha formattato: Colore carattere: Automatico

Formattato: Interlinea: 1,5 righe

ha formattato: Colore carattere: Automatico

diffusion of IGE-CFA record (Appendix D, Fig. D1). This ensures that our approach accurately reflects the discrete signal and validates the effectiveness of the mixing length quantification through step function.



95 Figure 8. PSD of continuous and back-diffused data compared to discrete spectrum for a) ISP-UNIVE, b) LSCE, and c) IGE. The crossing point of the dot lines, representative of the nearly flat white noise (ε_N) and the signal (S), corresponds at the SNR=1. For each system, the shading areas represent the period range at which the diffusion in firn (yellow), mixing in the CFA (orange) and measurement noise (brown) dominate.

4 Discussion

605

610

The comparison of isotopic continuous and discrete records from the 4-m PALEO2 firn core highlights the advantages and limitations of the operating procedures and technical features of three CFA-CRDS systems developed at ISP-UNIVE, LSCE, and IGE (Tab. 6). We confirm that the primary advantage of the continuous method is itsRegarding its time efficiency-time efficiency. Use using the LSCE-CFA system, we were able to analyse the 18 m PALEO2 firm core in two days (Fig. 9). The cutting of the sticks was done in parallel to the melting, avoiding the storage of the firn for extended period of time and allowing for immediate resampling if needed. In contrast, discrete processing and analysis at 1.5 cm of the 4-m core section took over a month. Extrapolating this analytical payload, analysing the entire PALEO2 core would take more than five months. A notable limitation of the CFA setup is its application to the low-density upper part of the cores (specifically, the upper 1.672 m for the PALEO2 core), where challenges in controlling melting speed and stick collapse require the use of discrete measurements rather than CFA. As previously found at the other institutes CFA equipped institutes with a CFA, the precision for discrete and continuous flow analyses are equivalent (Emanuelsson et al., 2015; Gkinis et al., 2011; Jones et al., 2017a). Here, by using PSD to evaluate the effective resolution imposed by measurement noise, in addition to solely the precision, we were able to determine the resolution at which records can be interpreted: 1.8 cm, 1.6 cm and 1.3 cm for ISP-UNIVE, LSCE and IGE, respectively. The primary factors affecting the precision and the resolution are the performance of the Picarro instrument and

the humidity level maintained during the analysis. Indeed, by setting the effective resolution at which the impact of mixing can be removed from the signal, using an instrument with better precision will directly improve the signal. For instance, implementing a VCOF-CRDS instrument with 20-fold better precision (Casado et al., 2024) could reach millimetric effective resolution.

-Maintaining a constant high humidity level is crucial for mitigating performance variations (Davidge et al., 2022), as this was identified as the key factor responsible for the difference between the ISP-UNIVE-CFA and discrete results. Additionally, the CFA method is limited by mixing within the system which smooth the measured signal. In this study, we focused and presented results relative to firm cores. However, the impact of diffusivity may differ in deeper and denser sections of the ice core due to variations in ice porosity. Furthermore, changes in melt-head temperature and melt rate settings for denser core analyses may also influence the mixing impact. Therefore, additional tests are needed to accurately characterise mixing in deeper ice. Additionally, the CFA method can be limited by mixing within the system, requiring signal integration over several millimeters of depth to accurately reflect the isotopic composition of the ice.

620

625

We validated the mixing lengths evaluated by step function through PSD analysis of the back-diffused profile for each of the three systems, confirming that the σ_{mix} derived from ice-to-firn, firn-to-ice, and ice-to-ice transitions serves as a reliable surrogate for the realistic case of firn-to-firn transitions. Furthermore, although our study focused on low-density firn cores, we expect these findings to remain valid - or potentially improve - for deeper core sections, given the reduced mixing that is likely to occur at the melt-head levelstage. The IGE-CFA system, characterised by longer distribution line, a 1,000 μ l volume debubbler, and two dust filters, results in the longer σ_{MH} (1.8±0.3 cm). However, this increased mixing length is compensated by the low noise level of the high-performance analyser, which enhances effective resolution.

Back-diffusion can effectively mitigate the mixing effect at high frequencies. However, while the corrected data show a \sim 0.1 ‰ gain in isotopic signal in proximity of the climatic peaks, the improvement compared to the discrete profile is very limited. This is consistent with the PSD of both continuous and discrete records, where the signal is dominated by longer periods (20–

100 cm, with a power of 10⁻¹-10⁰ ‰² m); while at mixing scale (10–20 cm) it is associated with lower power (10⁻³-10⁻⁴ ‰² m) comparable to the instrumental limit. These findings suggest that the impact of back-diffusion correction is limited for cores recording inter-annual to decadal signals (Casado et al., 2020; Münch & Laepple, 2018). However, it may become crucial in high accumulation areas for records with greater variability at shorter depth scales, such as deeper core sections where decadal signals are compressed into smaller depths. It is also relevant when analysing significant events, like those associated with atmospheric rivers (Wille et al., 2022), in areas where firm diffusion does not significantly erase the signal, unlike at the PALEO site. Furthermore, removing the effects of firm diffusion occurring prior to ice core drilling will require the application of back-diffusion function, along with accurate estimates of variability on centimetric scales (Jones et al., 2017b).

The LSCE-CFA, characterised by the lower discrepancy compared to discrete results (Fig. 7 e and f), has a maximum potential resolution of 0.7 cm, according to the mixing length. However, the actual achievable resolution for this specific measurement campaign is limited to 1.6 cm due to the relatively low performance of the vaporiser-Picarro system. This suggests that using a better Picarro analyser, characterised in particular by a better Allan variance, could significantly improve the LSCE-CFA

setup's performance. Here, we argue that the signal measured with the LSCE-CFA from the PALEO2 firn core (Fig. 9) accurately reflects the isotopic variability present in the firm, both in terms of δ^{18} O and d-excess. Furthermore, the results obtained can be confidently compared to cores measured at the other institutes.

An additional limitation of CFA systems is data loss at the beginning and end of the analysis due to the memory effect of the CRDS analyser. We strongly recommend using an ice stick with an isotopic composition similar to that of the samples before and after the analysis rather than mock UPW ice, as recently suggested by Davidge et al. (2022). For firn analysis, filling the tubes with depleted water of similar isotopic composition to that of the core helps mitigate transitions at the MH during the switch from ice to firn. Since memory effects decay exponentially, the length of data that must be removed to eliminate this effect depends on the isotopic composition difference. At IGE, a mock UPW ice with δ^{18} O composition of -12% precedes ice core analyses. For a δ^{18} O difference of about 40% between mock and sample ice, approximately 9.5 cm of the record must be removed. Conversely, for an ice stick with δ^{18} O difference of 3-4%, only the first 1.8 cm are affected by memory effect. To ensure reliable isotopic records, we list recommendations for future improvement or setting up of a CFA-CRDS system:

- First, developing a short transport line and then selecting a low-volume debubbler can reduce mixing.
- Installing conductivity devices both downstream of the MH and upstream of the CRDS instrument ensures accurate
 depth-scale attribution.
- Using ice sticks or filling the tubes with water of isotopic composition similar to the samples, rather than UPW ice, helps reduce memory effects. In addition, avoiding the use of UPW water in the system during the analysis for to clean the line minimises data loss (Dallmayr et al., 2024).
- Conduct pre-analysis testing of the core density to determine the appropriate MH temperature for achieving the
 desired flow rate and select a melting rate that allows a long integration time to enhance measurement precision.
- Maintain constant high humidity levels for isotope analysis (optimal range for the Picarro instrument: 18,000-22,000 ppmv) mitigates performance variations (Davidge et al., 2022; Gkinis et al., 2010).

Table 6. Summary of the main advantages and limitations identified in the CFA-CRDS comparison.

	Values	Comments
Advantages		
Time efficiency	1.5-1.8 m h ⁻¹	CFA reduces the time needed to analyse deeper ice cores.
Precision	$0.02\text{-}0.05\text{_}\%$ for $\delta^{18}\text{O}$, $0.06\text{-}0.16\text{_}\%$ for δD	The precision is primarily related to Picarro performance and secondarily by the humidity level maintained during analysis. The optimum level for Picarro is 18,000-22,000 ppmv.
High-resolution	1.3-1.8 cm	The limit resolution is primarily determined by the measurement noise.
Limits		
Mixing	0.7-2 cm	The mixing effect can be restored at a period of about 5 cm. The error introduce is 0.06 % for δ^{18} O.

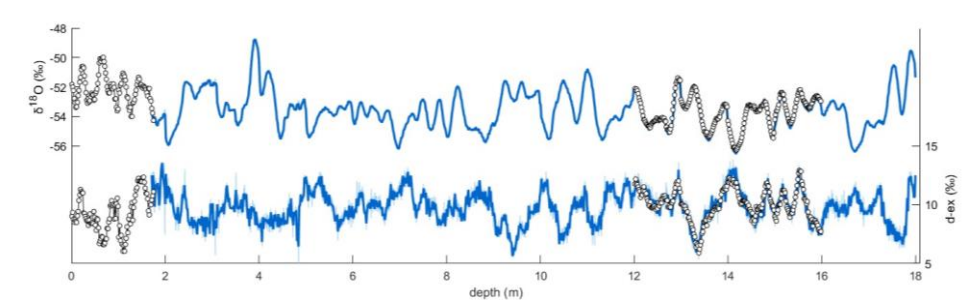


Figure 9. The 18 m PALEO2 core analysed with CFA-CRDS system at LSCE. The δ^{18} O and d-excess profiles of the raw data (light blue) and block-averaged at 1.6 cm data (blue) are shown with the discrete results (white dots).

5 Conclusions

The technical intercomparison of the three CFA-CRDS systems developed at the ISP-UNIVE, LSCE and IGE, highlighted each system's strengths and identified opportunities for future optimisation and development. Operating at a melt rate of 2.5-3 cm min⁻¹ under stable conditions, these systems measure 8-10 m of firn core per day, confirming that CFA-CRDS is a fast, high-resolution method for isotope analysis, with precision comparable to the discrete method. For ISP-UNIVE-CFA and LSCE-CFA systems, the main limitation in achieving higher resolution is imposed by the performance of the analyser. Conversely, the IGE-CFA system, with the great advantage of providing chemistry measurements online, has the setup limitation related to its longer distribution line and higher volume debubbler, which promotes mixing. To optimise system performance, it is crucial to set a melt rate high enough to ensure sufficient flow for all instruments and fraction collectors in the CFA system, while minimising excessive mixing at the melt-head and in the tubing, and without extending the duration of the CFA campaign for melting the core. At the same time, the melt rate must not be too high, as this would require shorter integration times—thereby compromising precision—and resulting in mixing affecting longer depth intervals, when it is converted from seconds to centimeters.

Finally, the outcomes of this work gave the basis for the post-processing of four PALEO cores analysed at ISP-UNIVE, LSCE, and IGE as part of the EAIIST (Traversa et al., 2023), allowing the climate signal to be interpreted by reconstructing it at the highest retrievable resolution.

Appendix A: Allan Variance for different humidity levels ranging from 10 to 20,000 ppmv

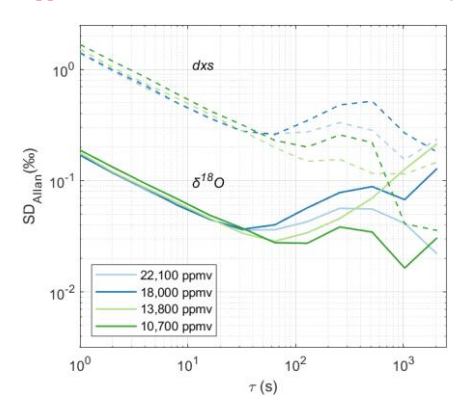


Figure A1. δ^{18} O and d-excess Allan Variance computed from 1-hour continuous UPW flow for humidity levels ranging from 10,000 to 20,000 ppmv.

Table A2. Allan Variance for δ^{18} O, δ D and d-excess concerning the integration times (τ) needed to melt 0.1 cm and 1.5 cm of the ice core at the melting rate of 3 cm min⁻¹.

	SD 0.1 cm		SD 1.5 cm			
$\delta^{18}O$ (‰)	<u>δD (‰)</u>	<u>dxs (‰)</u>	$\delta^{18}O$ (%)	<u>δD (‰)</u>	<u>dxs (‰)</u>	
0.12	0.35	1.10	0.04	0.13	0.32	

700 Appendix B: continuous measurement of UPW

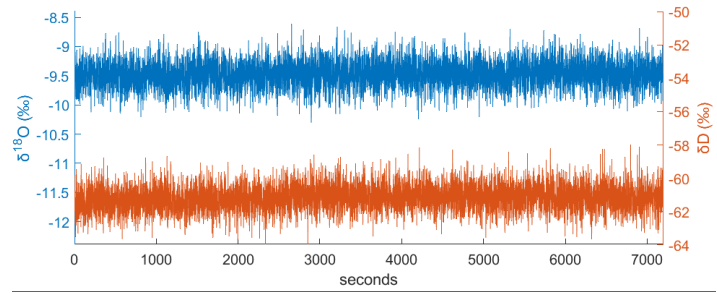


Figure B1. δ^{18} O and δ D results from a 2-hour continuous injection of UPW at ISP-UNIVE (~14,000 ppmv).

AAppendix CB: mixing lengths evaluated at MH and SV levelsstages

Table CB1. δ^{18} O mean mixing lengths (σ_{MH}) at level-stage of the melt-head derived from the normal PDF calculated for N number of firn-to-ice, ice-to-firn and ice-to-ice isotopic steps. The σ_{MH} is the mean value of all the steps for each institute. The lengths are expressed in mm accounting for the nominal melting speed and the respective 1SD are in parenthesis. The σ_{SV} is obtain from the steps at selector valve levelstage.

	σ _{MH} firn-ice (mm)		σ _{MH} ice-firn (mm)		σ _{MH} ice-ice (mm)		σ_{MH} (mm) σ_{SV} (s)		5sv (s)
ISP-UNIVE	N=4	10.5 (0.6)	N=3	12.2 (0.3)		-	11.2 (1.0)	N=4	20.0 (0.6)
LSCE	N=2	8.4 (0.1)		-	N=5	6.4 (0.5)	7.1 (0.1)	N=4	8.6 (1.4)
IGE		-	N=6	18.2 (3.0)		-	18.2 (3.0)	N=8	16.8 (2.3)

Appendix D←: CRDS processed data at 0.5 cm in comparison with record constructed at 1.5 cm and discrete data

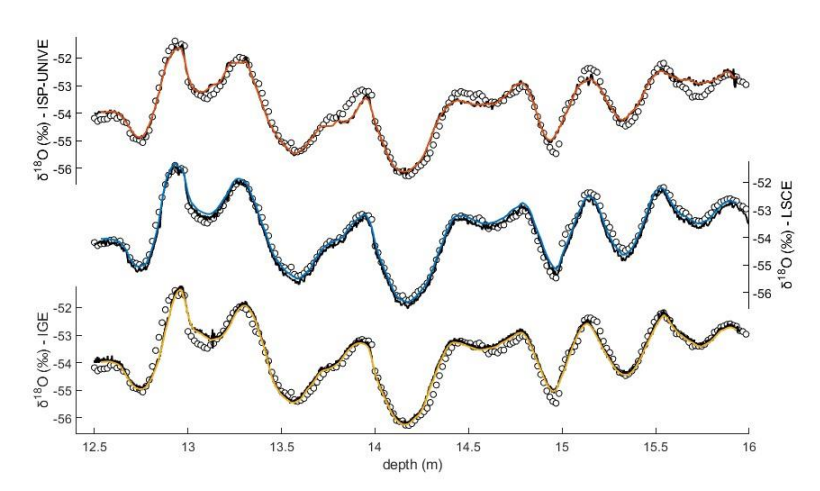


Figure $\overline{DC}1$. Comparison of $\delta^{18}O$ from CFA post-processed data at 0.5 cm resolution (black lines) and discrete values (white dots). Colored lines show discrete records constructed from CFA measurements at a 1.5 cm resolution, after calibration correction.

Appendix ED: X-axis melt rate values and associated standard deviations

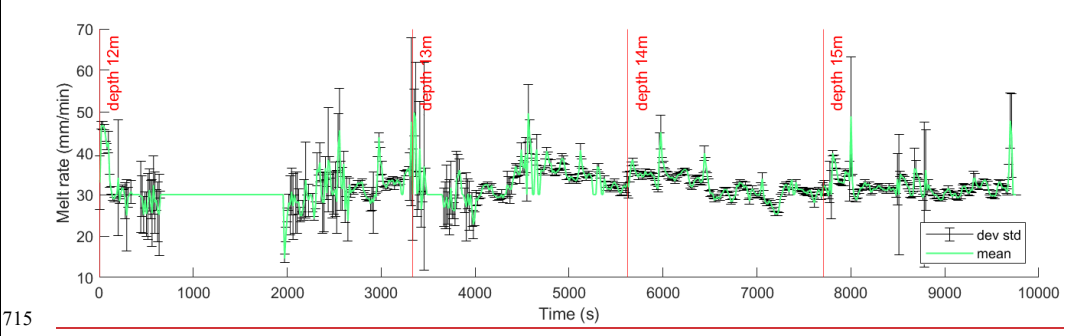


Figure E1. Mean melt rate variations and associated standard deviations computed over ~15 s intervals from the IGE dataset, corresponding to an approximate depth resolution of 0.5 cm.

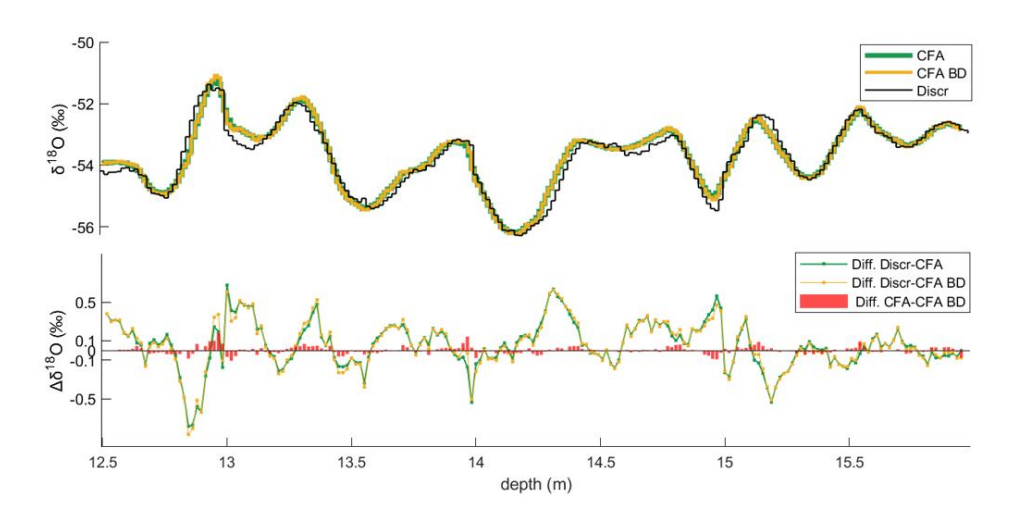
Appendix FE: Sensitivity test of the evaluation of the mixing length

720

725

Back-diffusion can mitigate the mixing effect at higher frequencies. To quantify the gain in isotopic composition, we present the continuous $\delta^{18}O$ IGE profile back-diffused with $\sigma_{mix}=1.8\pm0.3$ cm (Fig. D1). To prevent amplification of measurement noise, high frequencies with a signal-to-noise ratio (SNR) below 1 are removed by block averaging the profile at the specified frequency limit. Block averaging aggregates isotope records onto a new depth scale resolution, defined by each system's frequency limit. The original data are averaged within each interval and assigned to the corresponding depth point on the new scale. When comparing the raw data and the back-diffused profiles, we observe a gain of up to 0.1 % in proximity of the climatic peaks. However, since trough PSD analysis both continuous and discrete records show very low power at mixing length scale compared to the power of the dominant signal, it is evident that the back-diffusion approach has a limited impact on restoring the signal, when compared to the discrete profile.

ha formattato: Inglese (Regno Unito)



[730 Figure Fe1. (Top) Discrete δ¹⁸O record (black) compared with IGE-CFA profile (green) and back-diffused profile using σ_{mix}= 1.8 cm (yellow). (Bottom) The difference between discrete record and the original CFA profile (green) and the back-diffused profile (yellow line). Red bars represent the difference between CFA and back-diffused data.

Author contributions

AP, AS, DZ and JG developed the ISP-UNIVE-CFA-CRDS and performed the measurement in Venice; EF, RJ, OJ, AL developed the LSCE-CFA-CRDS system; AP, EF, RJ, TT and MC performed the measurement in Paris; EG, PDA, FP, JS and PG developed the IGE-CFA-CRDS and performed the measurement in Grenoble; AP and MC analysed the data and wrote the manuscript draft; EF, PDA, AL, AS, EG, CM, JS and BS reviewed and edited the manuscript. JS designed and supervised the EAIIST project.

Competing interests

740 The authors declare that they have no conflict of interest.

Acknowledgements

We thank the research groups at ISP-UNIVE, LSCE and IGE for their technical support and the resources made available for the analyses in their laboratories. We acknowledge the ANR EAIIST project, grant ANR—16-CE01-0011-01 of the French

Agence Nationale de la Recherche, the BNP-Paribas foundation and its Climate Initiative Program, the Institut Polaire Français

IPEV, the MIUR (Ministry of Education, University and Research) - PNRA (National Antarctic Research Program) through
the "EAIIST" PNRA16_00049-B and "EAIIST-phase2" PNRA19_00093 projects. We thank the MPM logistic team from
Seriate for the special transportation of the processed ice samples.

Financial support

This work was supported by the Polar Science PhD scholarship from Ca' Foscari University of Venice and the Erasmus+program.

References

750

755

- Alley, R. B.: Ice-core evidence of abrupt climate changes, Proc. Natl. Acad. Sci. USA, 97, 1331–1334, https://www.pnas.org/doi/full/10.1073/pnas.97.4.1331, 2000.
- Barbaro, E.: Fast liquid chromatography coupled with tandem mass spectrometry for the analysis of vanillic and syringic acids in ice cores, unpublished manuscript or conference presentation, 2022.
- Casado, M., Münch, T., and Laepple, T.: Climatic information archived in ice cores: impact of intermittency and diffusion on the recorded isotopic signal in Antarctica, Clim. Past, 16, 1581–1598, https://doi.org/10.5194/cp-16-1581-2020, 2020.
- Casado, M., Landais, A., Picard, G., Arnaud, L., Dreossi, G., Stenni, B., and Prié, F.: Water isotopic signature of surface snow metamorphism in Antarctica, Geophys. Res. Lett., 48, e2021GL093382, https://doi.org/10.1029/2021GL093382, 2021.
 - Casado, M., Landais, A., Stoltmann, T., Chaillot, J., Daëron, M., Prié, F., et al.: Reliable water vapour isotopic composition measurements at low humidity using frequency-stabilised cavity ring-down spectroscopy, Atmos. Meas. Tech., 17, 4599–4612, https://doi.org/10.5194/amt-17-4599-2024, 2024.
- 765 Craig, H.: Isotopic exchange effects in the evaporation of water: 1. Low-temperature experimental results, J. Geophys. Res., 68, 5079–5087, https://agupubs.onlinelibrary.wiley.com/doi/abs/10.1029/jz068i017p05079, 1963.
 - Crotti, I., Quiquet, A., Landais, A., Stenni, B., Wilson, D., Severi, M., et al.: TALDICE high resolution measurements of δ18O, d-excess and ssNa+ fluxes for MIS 5.5, MIS 7.5 and MIS 9.3 [dataset bundled publication], https://doi.org/10.1594/PANGAEA.941857, 2022.
- 770 Dallmayr, R., Meyer, H., Gkinis, V., Laepple, T., Behrens, M., Wilhelms, F., and Hörhold, M.: Assessment of Continuous Flow Analysis (CFA) for High-Precision Profiles of Water Isotopes in Snow Cores, EGUsphere [preprint], https://doi.org/10.5194/egusphere-2024-1807, 2024.
 - Dansgaard, W.: Stable isotopes in precipitation, Tellus B, 16, 436-468, 1964.
 - Davidge, L., Steig, E. J., and Schauer, A. J.: Improving continuous-flow analysis of triple oxygen isotopes in ice cores: insights from replicate measurements, Atmos. Meas. Tech., 15, 7337–7351, https://doi.org/10.5194/amt-15-7337-2022, 2022.
 - Emanuelsson, B. D., Baisden, W. T., Bertler, N. A. N., Keller, E. D., and Gkinis, V.: High-resolution continuous-flow analysis setup for water isotopic measurement from ice cores using laser spectroscopy, Atmos. Meas. Tech., 8, 2869–2883, https://doi.org/10.5194/amt-8-2869-2015, 2015.
- Genthon, C., Piard, L., Vignon, E., Madeleine, J.-B., Casado, M., and Gallée, H.: Atmospheric moisture supersaturation in the near-surface atmosphere at Dome C, Antarctic Plateau, Atmos. Chem. Phys., 17, 691–704, https://doi.org/10.5194/acp-17-691-2017, 2017.
 - Gkinis, V., Popp, T. J., Johnsen, S. J., and Blunier, T.: A continuous stream flash evaporator for the calibration of an IR cavity ring-down spectrometer for the isotopic analysis of water, Isot. Environ. Health Stud., 46, 463–475, https://doi.org/10.1080/10256016.2010.538052, 2010.

- 785 Gkinis, V., Popp, T. J., Blunier, T., Bigler, M., Schüpbach, S., Kettner, E., and Johnsen, S. J.: Water isotopic ratios from a continuously melted ice core sample, Atmos. Meas. Tech., 4, 2531–2542, https://doi.org/10.5194/amt-4-2531-2011, 2011
 - Gkinis, V., Popp, T. J., Blunier, T., Bigler, M., Schüpbach, S., and Johnsen, S. J.: Water isotopic ratios from a continuously melted ice core sample, Atmos. Meas. Tech. Discuss. [preprint], https://doi.org/10.5194/amtd-4-4073-2011, 2011.
- 790 Gkinis, V., Holme, C., Kahle, E. C., Stevens, M. C., Steig, E. J., and Vinther, B. M.: Numerical experiments on firn isotope diffusion with the Community Firn Model, J. Glaciol., 67, 450–472, https://doi.org/10.1017/jog.2021.1, 2021.
 - Goursaud, S., Masson-Delmotte, V., Favier, V., Preunkert, S., Fily, M., Gallée, H., et al.: A 60-year ice-core record of regional climate from Adélie Land, coastal Antarctica, Cryosphere, 11, 343–362, https://doi.org/10.5194/tc-11-343-2017, 2017.
- 795 Grisart, A., Casado, M., Gkinis, V., Vinther, B., Naveau, P., Vrac, M., et al.: Sub-millennial climate variability from high-resolution water isotopes in the EPICA Dome C ice core, Clim. Past, 18, 2289–2301, https://doi.org/10.5194/cp-18-2289-2022, 2022.

800

805

- Huybrechts, P., Rybak, O., Pattyn, F., Ruth, U., and Steinhage, D.: Ice thinning, upstream advection, and non-climatic biases for the upper 89% of the EDML ice core from a nested model of the Antarctic ice sheet, Clim. Past, 3, 577–589, https://doi.org/10.5194/cp-3-577-2007, 2007.
- Johnsen, S. J., Clausen, H. B., Cuffey, K. M., Hoffmann, G., and Creyts, T. T.: Diffusion of stable isotopes in polar firn and ice: the isotope effect in firn diffusion, in: Physics of Ice Core Records, edited by: Hondoh, T., Hokkaido University Press, 121–140, https://doi.org/10.7916/D8KW5D4X, 2000.
- Jones, T. R., White, J. W. C., Steig, E. J., Vaughn, B. H., Morris, V., Gkinis, V., et al.: Improved methodologies for continuous-flow analysis of stable water isotopes in ice cores, Atmos. Meas. Tech., 10, 617–632, https://doi.org/10.5194/amt-10-617-2017, 2017.
- Jones, T. R., Cuffey, K. M., White, J. W. C., Steig, E. J., Buizert, C., Markle, B. R., et al.: Water isotope diffusion in the WAIS Divide ice core during the Holocene and last glacial, J. Geophys. Res.-Earth Surf., 122, 290–309, https://doi.org/10.1002/2016JF003938, 2017.
- 810 Laepple, T., Werner, M., and Lohmann, G.: Synchronicity of Antarctic temperatures and local solar insolation on orbital timescales, Nature, 471, 91–94, https://doi.org/10.1038/nature09825, 2011.
 - Laepple, T., Münch, T., Casado, M., Hoerhold, M., Landais, A., and Kipfstuhl, S.: On the similarity and apparent cycles of isotopic variations in East Antarctic snow pits, Cryosphere, 12, 169–187, https://doi.org/10.5194/tc-12-169-2018, 2018
- 815 Landais, A. and Stenni, B.: Water stable isotopes (δD, δ¹8O) from EPICA Dome C ice core (Antarctica) (0–800 ka), PANGAEA [data set], https://doi.org/10.1594/PANGAEA.934094, 2021.
 - Landais, A., Casado, M., Prié, F., Magand, O., Arnaud, L., Ekaykin, A., et al.: Surface studies of water isotopes in Antarctica for quantitative interpretation of deep ice core data, C. R. Geosci., 349, 139–150, https://doi.org/10.1016/j.crte.2017.05.003, 2017.
- 820 Lilien, D. A., Steinhage, D., Taylor, D., Parrenin, F., Ritz, C., Mulvaney, R., et al.: Brief communication: New radar constraints support presence of ice older than 1.5 Myr at Little Dome C, Cryosphere, 15, 1881–1888, https://doi.org/10.5194/tc-15-1881-2021, 2021.
 - Markle, B. R., Steig, E. J., Buizert, C., Schoenemann, S. W., Bitz, C. M., Fudge, T. J., et al.: Global atmospheric teleconnections during Dansgaard–Oeschger events, Nat. Geosci., 10, 36–40, https://doi.org/10.1038/ngeo2848, 2017
 - Münch, T. and Laepple, T.: What climate signal is contained in decadal- to centennial-scale isotope variations from Antarctic ice cores?, Clim. Past, 14, 2053–2070, https://doi.org/10.5194/cp-14-2053-2018, 2018.
 - Parrenin, F., Cavitte, M. G. P., Blankenship, D. D., Chappellaz, J., Fischer, H., Gagliardini, O., et al.: Is there 1.5-million-year-old ice near Dome C, Antarctica?, Cryosphere, 11, 2427–2437, https://doi.org/10.5194/tc-11-2427-2017, 2017.
- 830 Petit, J. R.: A detailed study of snow accumulation and stable isotope content in Dome C (Antarctica), J. Geophys. Res.-Oceans, 87, 4301–4312, https://doi.org/10.1029/JC087iC06p04301, 1982.
 - Petit, J. R.: Climate and atmospheric history of the past 420,000 years from the Vostok ice core, Antarctica, Nature, 399, 429–436, https://www.nature.com/articles/20859, 1999.

- Picard, G., Arnaud, L., Caneill, R., Lefebvre, E., and Lamare, M.: Observation of the process of snow accumulation on the
 Antarctic Plateau by time lapse laser scanning, Cryosphere, 13, 1983–1999, https://doi.org/10.5194/tc-13-1983-2019,
 2019
 - Sigl, M., Fudge, T. J., Winstrup, M., Cole-Dai, J., Ferris, D., McConnell, J. R., et al.: The WAIS Divide deep ice core WD2014 chronology Part 2: Annual-layer counting (0–31 ka BP), Clim. Past, 12, 769–786, https://doi.org/10.5194/cp-12-769-2016, 2016.
- 840 Steig, E. J.: Seasonal precipitation timing and ice core records, Science, 266, 1885–1886, https://doi.org/10.1126/science.266.5192.1885, 1994.

845

- Traversa, G., Fugazza, D., and Frezzotti, M.: Megadunes in Antarctica: migration and characterization from remote and in situ observations, Cryosphere, 17, 427–444, https://doi.org/10.5194/tc-17-427-2023, 2023.
- Wahl, S. K.: Atmosphere–snow exchange explains surface snow isotope variability, Geophys. Res. Lett., 49, e2022GL099529, https://doi.org/10.1029/2022GL099529, 2022.
- Wesche, C., Weller, R., König-Langlo, G., Fromm, T., Eckstaller, A., Nixdorf, U., and Kohlberg, E.: Neumayer III and Kohnen Station in Antarctica operated by the Alfred Wegener Institute, J. Large-Scale Res. Facil., 2, A85, https://doi.org/10.17815/jlsrf-2-152, 2016.
- Whillans, I. M. and Grootes, P. M.: Isotopic diffusion in cold snow and firn, J. Geophys. Res.-Atmos., 90, 3910–3918, https://doi.org/10.1029/JD090iD02p03910, 1985.
- Wille, J. D., Favier, V., Jourdain, N. C., Kittel, C., Turton, J. V., Agosta, C., et al.: Intense atmospheric rivers can weaken ice shelf stability at the Antarctic Peninsula, Commun. Earth Environ., 3, 14, https://doi.org/10.1038/s43247-022-00422-9, 2022.